Steady-state entanglement of spin qubits mediated by non-reciprocal and chiral magnons

Martijn Dols,^{1,*} Mikhail Cherkasskii,¹ Victor A. S. V. Bittencourt,² Carlos Gonzalez-Ballestero,³ Durga B. R. Dasari,⁴ and Silvia Viola Kusminskiy^{1,5,†}

¹Institute for Theoretical Solid State Physics, RWTH Aachen University, 52074 Aachen, Germany
²Institut de Science et d'Ingénierie Supramoléculaires (ISIS,
UMR7006), Université de Strasbourg, 67000 Strasbourg, France

³ Institute for Theoretical Physics and Vienna Center for Quantum Science and Technology, TU Wien, 1040 Vienna, Austria
⁴3. Physikalisches Institut, ZAQuant, University of Stuttgart, Allmandring 13, 70569 Stuttgart, Germany

⁵ Max Planck Institute for the Science of Light, Staudtstraβe 2, 91058 Erlangen, Germany

(Dated: September 17, 2025)

We propose a hybrid quantum system in which a magnet supporting non-reciprocal magnons, chiral magnons, or both mediates the dissipative and unidirectional coupling of spin qubits. By driving the qubits, the steady state of this qubit-qubit coupling scheme becomes the maximally entangled Bell state. We devise a protocol where the system converges to this entangled state and benchmark it including qubit decay and dephasing. The protocol is numerically tested on a hybrid system consisting of nitrogen-vacancy (NV) centers coupled to magnon surface modes of an yttrium iron garnet (YIG) film. We show that the dephasing time of the NV centers forms the bottleneck for achieving the entanglement of NV centers separated by a distance exceeding microns. Our findings identify the key technological requirements and demonstrate a viable route toward steady-state entanglement of solid-state spins over distances of several microns using magnonic quantum networks, expanding the toolbox of magnonics for quantum information purposes.

I. INTRODUCTION

The capability of tailoring and controlling the interactions between quantum emitters (QEs) is an essential requisite for functional quantum networks. Such interactions can be engineered to yield unidirectional coupling. where two QEs couple asymmetrically to each other such that the dynamics of one QE influences the other, but not the other way around [1, 2] This type of coupling can be harnessed to design quantum networks in which information flows in only one direction, with advantages for applications in information processing [3, 4]. In particular, it can be used for the generation of steady-state entanglement [5, 6], which is not achievable for the bidirectional equivalent [7, 8]. Achieving high-fidelity entanglement is a required resource for quantum information protocols such as cryptography [9], error correction [10, 11] and teleportation [12]. (Uni)directional coupling can be realized via modes exhibiting direction-dependent polarization [3] combined with QEs exhibiting polarizationdependent transitions. Such setup has been realized for example in quantum optics, by coupling atoms and quantum dots to waveguides and cavities tailored to exhibit fields with direction-locked polarization [13–22].

The integration of optical systems typically constraints some of the tunability of the hybrid system [23]. A promising alternative seeks to incorporate magnons, i.e. the quanta of spin waves in magnetic systems, as information carries exhibiting in-situ tunability as well as scal-

ability to nanoscale devices [24–29]. Magnons can be integrated seamlessly in hybrid systems since they can be coherently coupled to a vast range of excitations, including phonons [30-35], microwaves [36-40], optical photons [41–45], superconducting circuits [46–51] and single spins systems [52–64]. Crucially to this work, magnons can show intrinsic non-reciprocity and chirality, which are two central ingredients to realize unidirectional coupling between QEs. Specifically, the magnetic potential of the spin waves can depend on the propagation direction. This has been demonstrated e.g. for surface spin waves in ferromagnetic slabs [65, 66], giving rise to the so-called field displacement non-reciprocity. Such surface waves are inherently also chiral, i.e. they exhibit polarization-direction locking. Spin waves can also exhibit a dispersion relation that is asymmetric with respect to the direction propagation, a phenomenon called frequency non-reciprocity. Systems possessing this trait include ferromagnetic ultra-thin layers [67–71], ferromagnetic nanotubes [72, 73], and ferromagnetic [74-79] and antiferromagnetic [80–84] multilayered structures. This gives rise to the question, whether protocols for unidirectionally coupled QEs can be realized on a hybrid system where the mediations are non-reciprocal and chiral magnons, instead of photons.

In this work, we demonstrate that the non-reciprocity and chirality of magnons can be exploited to generate steady-state entanglement between remote spin qubits. Specifically, we consider a hybrid system (Fig. 1) in which two spin qubits are coupled to the spin-wave modes of a magnetic material that supports non-reciprocal and chiral magnon propagation. Under continuous resonant driving of the qubits, the magnon-mediated interaction causes any initial two-qubit state to evolve toward a Bell

^{*} martijn.dols@rwth-aachen.de

[†] kusminskiy@physik.rwth-aachen.de

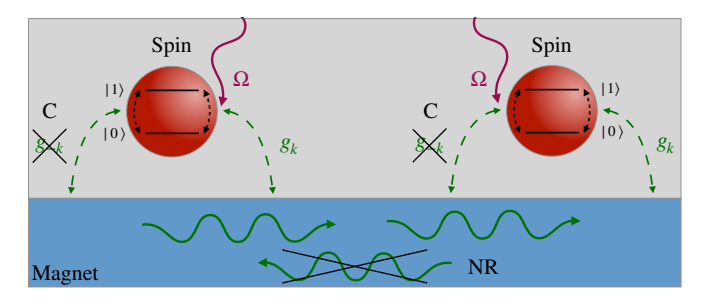


FIG. 1: Unidirectional coupling scheme between spin qubits mediated by magnons. The non-reciprocity (NR) of the magnet limits the propagation of the surface magnons to one propagation direction. Due to the chirality (C) the spin-magnon coupling g_k is non-vanishing only for one propagation direction of the magnons. The spin qubits are resonantly driven with a Rabi frequency Ω .

state, i.e. a maximally entangled state. The steady-state character of the generated entanglement is advantageous for quantum networking applications, because the target state is a stationary attractor of the dynamics rather than a transient state.

Building on the theoretical result, we consider a specific protocol to prepare the target state. We optimize the protocol by minimizing the time required to reach a given fidelity threshold, i.e. the time to approach the entangled state up to a set fidelity, and investigate the impact of intrinsic qubit relaxation and dephasing. Our analysis benchmarks the minimal dephasing and decay times required to achieve high-fidelity entangled states, providing guidelines for experimental design.

We assess a practical implementation of the proposed magnon-mediated entanglement scheme by considering a state-of-the-art platform: two NV-center qubits [85, 86] coupled via the magnetostatic surface magnons of a YIG film [53, 55, 61]. We find that high-fidelity entanglement can be achieved in this setup provided that (i) the separation of the NV centers is within the magnon coherence length, on the order of a few millimeters for YIG at low temperature [87], and (ii) the device is operated at cryogenic temperature, required to suppress thermal magnon population. Under these conditions, the main limitation for steady-state entanglement becomes the dephasing time of the NV centers. We find that a minimal dephasing time on the order of $T_{\phi} \sim 1.5 \,\mathrm{s}$ is required. This is an order of magnitude longer than the typical dephasing time of NV centers in current experiments, identifying the need for improved coherence preservation (e.g. via dynamical decoupling techniques [88]). Nevertheless, NV coherence times approaching the few-second regime have been reported [89], and further enhancements would make the envisioned entanglement protocol feasible.

The remainder of this work is structured as follows. In the first part of the manuscript we introduce the general concepts and the entangling protocol. In the second part we propose the physical implementation of the protocol using state-of-the-art magnetic platforms. Specifically, in Sec. II we show the derivation the unidirectional coupling of (spin) qubits mediated by a magnon bath. The proposed protocol and its benchmark of decoherence, as well as the benchmark of directional over unidirectional coupling, are introduced in Sec. III. We discuss the implementation of chiral magnons in Sec. IV A and of non-reciprocal magnons in Sec. IV B. In Sec. IV C, we consider a particular implementation consisting of NV centers and a YIG film. In Sec. V we present the conclusions and discuss possible alternative platforms.

II. MODEL

The low-energy excitations of magnetic systems are bosonic quasiparticles known as magnons. In the spinwave limit without considering magnon-magnon interaction terms, the Hamiltonian is generally given by

$$\hat{H}_M = \sum_{\mathbf{k}} \hbar \omega_{\mathbf{k}} \hat{m}_{\mathbf{k}}^{\dagger} \hat{m}_{\mathbf{k}}, \tag{1}$$

where the operator $\hat{m}_{k}^{(\dagger)}$ annihilates (creates) a magnon in mode k with frequency ω_{k} . The magnon modes and their dispersion depend on the geometry of the magnetic system considered.

We consider that magnons couple to identical qubits which are classically driven with a driving frequency ω_d and Rabi frequency Ω . The two states $|0\rangle$ and $|1\rangle$ of the qubits are separated by an energy $\hbar\omega_q$. In the rotating frame of the drive the Hamiltonian reads

$$\hat{H}_Q = \sum_i \hbar \delta_q \hat{\sigma}_i^+ \hat{\sigma}_i^- + \hbar \Omega(\hat{\sigma}_i^+ + \hat{\sigma}_i^-), \tag{2}$$

with the lowering operator $\hat{\sigma}^- = |0\rangle \langle 1|$, the raising operator $\hat{\sigma}^+ = (\hat{\sigma}^-)^{\dagger}$, and the detuning $\delta_q = \omega_q - \omega_d$.

The magnetic-field fluctuations generated by the magnons interact with the magnetic moment of the spin qubits, giving rise to a dipolar coupling. Under the rotating wave approximation (RWA), this resonant interaction is described by

$$\hat{H}_{\text{int}} = \sum_{i,\mathbf{k}} \hbar(g_{\mathbf{k},i}\hat{\sigma}_i^{\dagger}\hat{m}_{\mathbf{k}} + g_{\mathbf{k},i}^*\hat{m}_{\mathbf{k}}^{\dagger}\hat{\sigma}_i^{-}). \tag{3}$$

The directionality of the coupling is embedded in the coupling constants $g_{\mathbf{k},i}$. In a magnetic system, unidirectionality can arise due to chiral or unidirectional magnon transport, see Sec. IV. The consequence of both scenarios is that the qubits couple to only one specific propagation direction of the magnons, as visualized in Fig. 1, where the qubits are positioned along the axis where the time-reversal symmetry is broken [90], which we refer to as the unidirectional axis.

We derive the effective qubits' dynamics by tracing out the magnons within the Born-Markov approximation in App. A. Assuming that the magnons remain at zero temperature, we obtain an effective master equation describing the evolution of the qubits density operator $\hat{\rho}$, i.e. $\frac{\partial \hat{\rho}}{\partial t} = \mathcal{L}[\hat{\rho}]$, with the Liouvillian

$$\mathcal{L}[\hat{\rho}] = -\frac{i}{\hbar} \left([\hat{H}_Q, \hat{\rho}] + \hat{H}_{\text{eff}} \hat{\rho} - \hat{\rho} \hat{H}_{\text{eff}}^{\dagger} \right) + \hat{L} \hat{\rho} \hat{L}^{\dagger}, \qquad (4)$$

and an effective non-Hermitian Hamiltonian $\hat{H}_{\text{eff}} = \hat{H}_{\text{loc}} + \hat{H}_{\text{uni}}$.

The first term of this effective Hamiltonian describes the dissipation of the qubit due to the magnon bath

$$\hat{H}_{loc} = -i\hbar \sum_{i} \frac{J_q}{2} \hat{\sigma}_i^+ \hat{\sigma}_i^-, \tag{5}$$

where $J_q=2\pi\mathcal{D}(k_q)|g_{k_q}|^2/|v_{k_q}|$ is the magnon-mediated dissipative coupling constant. $\mathcal{D}(k)$ and $v_k=\partial\omega/\partial k$ are the magnonic density of states and the group velocity, respectively, evaluated at the wave number k_q which is in resonance with the qubit, i.e. $\omega_{k_q}=\omega_q$. Here, we assumed $v_{k_q}>0$ with the wave number defined along the unidirectional axis. This Hamiltonian acts locally on the qubits and hence does not lead to inter-qubit coupling.

The limitation of the coupling to only one propagation direction (chiral case), or the existence of only one propagation direction (non-reciprocal case), along the unidirectional axis generates a unidirectionality in the coupling between qubits, which is described by the second term of the effective Hamiltonian

$$\hat{H}_{\text{uni}} = -i\hbar \sum_{i>j} J_q e^{ik_q r_{i,j}} \hat{\sigma}_j^- \hat{\sigma}_i^+, \tag{6}$$

with the distance $r_{i,j} = r_i - r_j$ between qubit i and j. The ordering i > j of the qubits in Eq. (6) is dictated by the position along the unidirectional axis, such that $r_i > r_j$.

The last term of the Liouvillian in Eq. (4) corresponds to a quantum jump term with the Lindblad operator

$$\hat{L} = \sum_{i} \sqrt{J_q} e^{-ik_q r_i} \hat{\sigma}_i^{-}. \tag{7}$$

Eq. (4) is valid provided the Markov approximation is fulfilled, which is ensured by the conditions $\tau_m \ll \tau_q,\,\tau_{\delta,\Omega},$ where τ_m and τ_q are the correlation time of the magnon bath and of the spin qubit, respectively, and $\tau_{\delta,\Omega}=2/\sqrt{\delta^2+4\Omega^2}$ is the time constant associated with the driving of the qubit. Also, we assumed that the coupling between qubit i and j is instantaneous, which is valid for $|\delta_q|,\,J_q,\,\Omega,\ll v_{k_q}/r_{i,j}.$

The unidirectionality in the coupling between the qubits is best reflected when considering the time dynamics of the two-qubit initial states $|10\rangle$ and $|01\rangle$. As prescribed by Eq. (6), an excitation is only transferred from qubit 1 to qubit 2, if qubit 2 is located after qubit 1 on the unidirectional axis. Therefore, we expect that there is a transfer of quanta only for the initial state $|10\rangle$

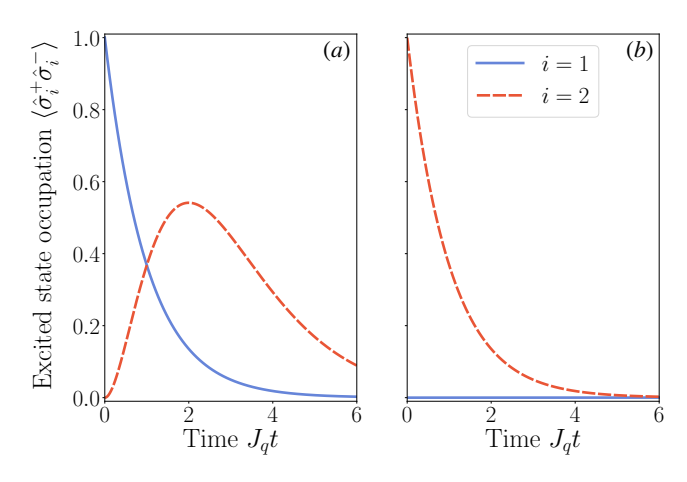


FIG. 2: Time dynamics according to the Liouvillian in Eq. (4) with initial state $|10\rangle$ in (a) and $|01\rangle$ in (b). The occupation of the excited state $\langle \hat{\sigma}_i^+ \hat{\sigma}_i^- \rangle$ of qubit i=1,2 is shown as a function of the time t normalized by the coupling J_q . For the input state $|10\rangle$ in (a), there is a transfer of excitation from qubit 1 to qubit 2, on top of the dissipation due to the bath. This transfer is lacking in (b), where the input state is $|01\rangle$, showing the unidirectionality of the coupling. In this figure, we set $J_q = 50\Omega$.

and not for $|01\rangle$. This expectation is confirmed in Fig. 2, where we plot the evolution in time of the excited state occupation according to Eq. (4). Due to the dissipative coupling given by Eq. (5), there will always be loss of the excitation of qubit i=1,2 on top of the unidirectional coupling.

We show the eigenstates of the Hamiltonian $\hat{H}_Q + \hat{H}_{\rm eff}$ for two qubits driven resonantly in App. B. We demonstrate that one of the eigenstates is in the null space of the Liouvillian, if the qubits are positioned along the unidirectional axis such that the distance between them satisfies $k_q r_{2,1} = 2\pi n$, for n integer. Therefore, this state $|\psi_s\rangle$ fulfills $\mathcal{L}[|\psi_s\rangle\langle\psi_s|] = 0$ and hence it is a dark state. Since this is the only state fulfilling the dark state condition, it is also the steady state. The existence of the steady state is guaranteed by the time-independence of the Liouvillian [91, 92]. For $J_q > 0$, the steady state takes the form

$$|\psi_s\rangle = \frac{1}{\sqrt{\zeta^2 + 1}} \left(i\zeta |00\rangle + \frac{1}{\sqrt{2}} (|10\rangle - |01\rangle) \right), \quad (8)$$

where $\zeta = J_q/(2\sqrt{2}\Omega)$ [5]. For $\zeta \ll 1$ the steady state corresponds to the maximally entangled Bell state $|\psi_-\rangle = (|10\rangle - |01\rangle)/\sqrt{2}$. Thus, for sufficiently large driving with respect to the dissipative coupling, the steady state is maximally entangled (and pure), contrary to its bidirectional equivalent [7, 8]. The parameter ζ controls the transient time t_s required to reach the steady state, such that $t_s \to \infty$ for $\zeta \to 0$ (see Fig. 9 in App. C).

III. PROTOCOL

We propose a protocol in which we let the state of two qubits separated by a distance $r_{2,1}$ with $k_q r_{2,1} = 2\pi n$ converge toward the entangled steady state given by Eq. (8). We take the initial state as $\hat{\rho}_{00} = |00\rangle \langle 00|$, since this is the steady state of the system without driving the qubits. After switching on the driving, we let this initial state evolve according to the Liouvillian in Eq. (4) for a given time t, giving the density matrix $\hat{\rho}(t)$. According to Eq. (8), the smaller ζ , the higher the entangled state fraction of the steady state. We quantify the overlap between $\hat{\rho}(t)$ and the entangled state $|\psi_-\rangle$ by calculating the fidelity $F(t) = \sqrt{\langle \psi_-|\hat{\rho}(t)|\psi_-\rangle}$ [12]. For sufficient time passed and for appropriately chosen ζ , the density matrix $\hat{\rho}(t)$ is such that the fidelity has exceeded a specific threshold F_T , i.e.

$$F(t) = \sqrt{\langle \psi_{-} | e^{\mathcal{L}t} [\hat{\rho}_{00}] | \psi_{-} \rangle} \ge F_{T}. \tag{9}$$

We denote the minimal time needed to fulfill this condition as the protocol time t_p .

To limit the effects of the intrinsic qubit dissipation, the protocol time should be minimized. Therefore, we vary ζ to find the minimal protocol time t_p to reach the fidelity threshold. One can see this optimization in Fig. 3(a) for $F_T=0.95$, 0.97 and 0.99. A smaller ζ comes with a larger entangled state $|\psi_-\rangle$ fraction, but also with a larger protocol time t_p , following the trend of the transient time t_s . Thus, a larger ζ is preferred. However, if ζ is too large, the overlap of the steady state and the entangled state $|\psi_-\rangle$ becomes too small to surpass the fidelity threshold F_T . This upper bound of ζ as a function of the fidelity threshold can be determined by solving the relation $F_T=|\langle \psi_s|\psi_-\rangle|$ for the threshold value ζ_T . This leads to

$$\zeta_T = \sqrt{\frac{1}{F_T^2} - 1}. (10)$$

Thus, a larger fidelity threshold corresponds to a lower upper bound ζ_T . Once ζ approaches the upper bound ζ_T , the protocol time increases. Since the overlap of the steady state and entangled state decreases for increasing ζ , the state of the system $\hat{\rho}(t)$ requires to have a higher overlap with the steady state, i.e. $\sqrt{\langle \psi_s | \hat{\rho}(t) | \psi_s \rangle}$, to surpass the fidelity threshold with the entangled state. A higher overlap of $\hat{\rho}(t)$ with the steady state typically corresponds to more time required (see also Fig. 9 in App. C). Thus, the protocol time increases for ζ close to ζ_T . This results in a competition leading to a nonmonotonic behavior of the protocol time t_p as a function of ζ , together with an upper bound on ζ , as shown in Fig. 3(a).

Varying F_T and iterating over all ζ , we compute the minimal protocol time t_p for each F_T . In Fig. 3(b) we examine this relation between the fidelity and the protocol time. As expected, a higher fidelity comes at the cost

of a higher protocol time. We investigate the effects of a variation in ζ on the protocol time and on the threshold fidelity in App. D.

A. Intrinsic qubit decoherence

Since spin qubits are intrinsically subject to dissipative processes, we investigate the effect of decay and dephasing of the spin qubits on the protocol. To include the former, we add the qubit decay $1/T_1 \sum_{i=1,2} \mathcal{D}[\hat{\sigma}_i^-]\hat{\rho}$, where T_1 is the qubit lifetime and

$$\mathcal{D}[\hat{A}]\hat{\rho} = \hat{A}\hat{\rho}\hat{A}^{\dagger} - \frac{1}{2}\left(\hat{A}^{\dagger}\hat{A}\hat{\rho} + \hat{\rho}\hat{A}^{\dagger}\hat{A}\right) \tag{11}$$

is the Lindblad dissipator. For a given fidelity threshold F_T , we increase T_1 and vary ζ until the fidelity threshold is surpassed, so that we obtain the minimal lifetime needed such that the protocol succeeds. The result is visualized in Fig. 3(c) with a blue solid line. We see that a higher threshold fidelity requires a higher lifetime. This is along the lines of the expectation, since a higher fidelity corresponds to a higher protocol time (see Fig. 3(a)) and hence the state has to be preserved for a longer time. In a similar fashion we obtain a benchmark of the dephasing time T_ϕ by adding the qubit dephasing $1/T_\phi \sum_{i=1,2} \mathcal{D}[\hat{\sigma}_i^+ \hat{\sigma}_i^-]\hat{\rho}$. Again, we vary T_ϕ until for any ζ the protocol converges. This results in the red dashed line in Fig. 3(c).

By comparing the lifetime T_1 and dephasing time T_{ϕ} in Fig. 3(c), we observe that the required lifetime is larger than the dephasing time for all fidelity thresholds F_T . Thus, a spin qubit with a decent lifetime is prioritized over dephasing time.

B. Directional coupling

In this subsection, we investigate the consequences of directional instead of unidirectional coupling of the qubits, which can happen when two magnon modes with wave numbers $k_{q,R}$ and $k_{q,L}$ fulfill the resonant condition $\omega_q = \omega_k$, see Sec. II. We consider group velocities $v_{k_{q,R}} > 0$ and $v_{k_{q,L}} < 0$, corresponding to propagation towards the left and right, respectively, along the unidirectional axis. Due to the difference in sign, the coupling of the qubits to these magnon modes is not unidirectional. We assume that the dissipative coupling $J_{q,j} = 2\pi \mathcal{D}(k_{q,j})|g_{k_q,j}|^2/|v_{k_q,j}|$ due to the coupling to the magnon modes $k_{q,R}$ and $k_{q,L}$ is such that $J_{q,R} > J_{q,L}$. Thus, the coupling is directional.

The directional coupling is described by the Liouvillian $\mathcal{L}_{\text{di}} = \mathcal{L}_Q + \mathcal{L}_{\text{uni},1} + \mathcal{L}_{\text{uni},2}$, where $\mathcal{L}_Q[\hat{\rho}] = -(i/\hbar)[\hat{H}_Q,\hat{\rho}]$ and

$$\mathcal{L}_{\mathrm{uni},j}[\hat{\rho}] = -\frac{i}{\hbar} \left(\hat{H}_{\mathrm{eff},j} \hat{\rho} - \hat{\rho} \hat{H}_{\mathrm{eff},j}^{\dagger} \right) + \hat{L}_{j} \hat{\rho} \hat{L}_{j}^{\dagger}, \qquad (12)$$

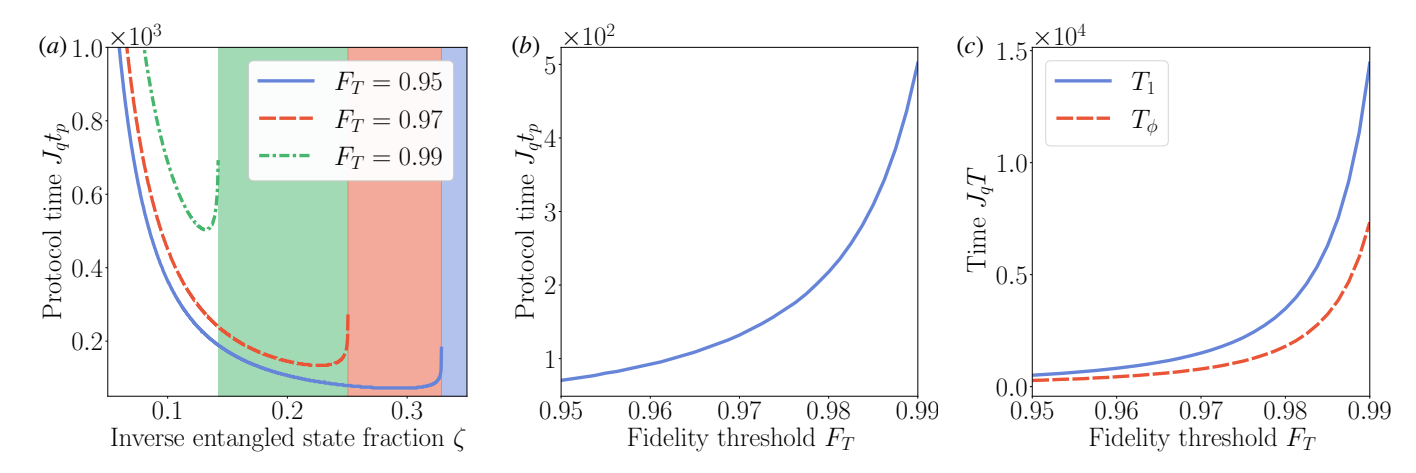


FIG. 3: (a) Protocol time t_p normalized by the coupling strength J_q as a function of $\zeta = J_q/(2\sqrt{2}\Omega)$ for different fidelity thresholds F_T . A larger ζ corresponds to a shorter protocol time t_p , up to the regime where the threshold condition of Eq. (9) imposes an upper bound on ζ , as given by Eq. (10) and indicated with a vertical line. A higher fidelity F_T requires a longer time t_p for a given ζ . (b) Protocol time t_p as a function of the fidelity threshold F_T . A higher fidelity comes at the cost of a longer time t_p . (c) Qubit lifetime T_1 and dephasing time T_ϕ normalized by the coupling strength J_q as a function of the fidelity threshold F_T . A higher fidelity F_T can be obtained at the expense of a longer required lifetime T_1 or dephasing time T_ϕ .

with effective Hamiltonian $\hat{H}_{\text{eff},j} = \hat{H}_{\text{loc},j} + \hat{H}_{\text{uni},j}$ and Lindblad operator

$$\hat{L}_{j} = \sum_{i=1,2} \sqrt{J_{q,j}} e^{-ik_{q,j}r_{i}} \hat{\sigma}_{i}^{-}.$$
 (13)

The first term of the effective Hamiltonian $\hat{H}_{\mathrm{eff},j}$ is the local Hamiltonian

$$\hat{H}_{\text{loc},j} = -i\hbar \sum_{i=1,2} \frac{J_{q,j}}{2} \hat{\sigma}_i^+ \hat{\sigma}_i^-.$$
 (14)

The second term $\hat{H}_{\mathrm{uni},j}$ describes the coupling of the qubits and depends on the propagation direction of the magnon mode, which for right-propagating magnons equals

$$\hat{H}_{\text{uni},R} = -i\hbar J_{q,R} e^{ik_{q,R}r_{2,1}} \hat{\sigma}_1^- \hat{\sigma}_2^+$$
 (15)

and for left-propagating

$$\hat{H}_{\text{uni},L} = -i\hbar J_{q,L} e^{ik_{q,L}r_{1,2}} \hat{\sigma}_1^+ \hat{\sigma}_2^-.$$
 (16)

Now, we investigate the consequences of the directional coupling for the protocol. As we found previously for right-propagating magnons, the qubits should be positioned such that $k_{q,R}r_{2,1}=2\pi n$, with n integer, although this condition is not very stringent as shown in App. E. However, this condition may not be fulfilled for left-propagating magnons with wave number $k_{q,L}$. Therefore, we vary both $J_{q,L}$ and $k_{q,L}$ and examine their effect on the protocol time $t_{p,\mathrm{di}}$. We do this in similar fashion to the unidirectional protocol case. We let the initial state $\hat{\rho}_{00}$ evolve in time according to the Liouvillian $\mathcal{L}_{\mathrm{di}}$ until the fidelity threshold F_T is surpassed. We show

the results in Fig. 4, where we took $F_T = 0.95$. Here, we see that for $J_{q,L}/J_{q,R} \lesssim 10^{-4}$ the coupling $J_{q,L}$ does not prevent the convergence for all wave numbers $k_{q,L}$, where the directional protocol time $t_{p,di}$ is similar to the unidirectional protocol time t_p . For larger $J_{q,L}$, the convergence depends on the wave number $k_{q,L}$. If the phase $k_{q,L}r_{2,1}$ is not close to zero, or equivalently, a multiple of 2π , then the fidelity threshold is not surpassed, which is indicated with white. Therefore, in the case of directional coupling, it is important to comply with this condition $k_{q,L}r_{2,1}=2\pi m$, with m integer. If this condition is met, the range of possible coupling strengths $J_{q,L}$ is vast as one can see in the inset of Fig. 4, where we take $k_{q,L}r_{2,1}=0$. For $J_{q,L}/J_{q,R}$ approaching 1, we see that at some point there is no convergence, as we expect from the bidirectional $(J_{q,R} = J_{q,L})$ case [7, 8].

IV. IMPLEMENTATION WITH MAGNETIC SYSTEMS

In this section we discuss in detail the implementation of the unidirectional coupling of single spins to chiral or non-reciprocal magnons, which we used in Sec. II. A schematic overview of possible physical mechanisms for unidirectional coupling in magnetic systems is given in Fig. 5. After discussing these mechanisms, we consider a specific hybrid system where this can be realized, consisting of NV centers coupled to the chiral and field displacement non-reciprocal surface waves of a YIG film.

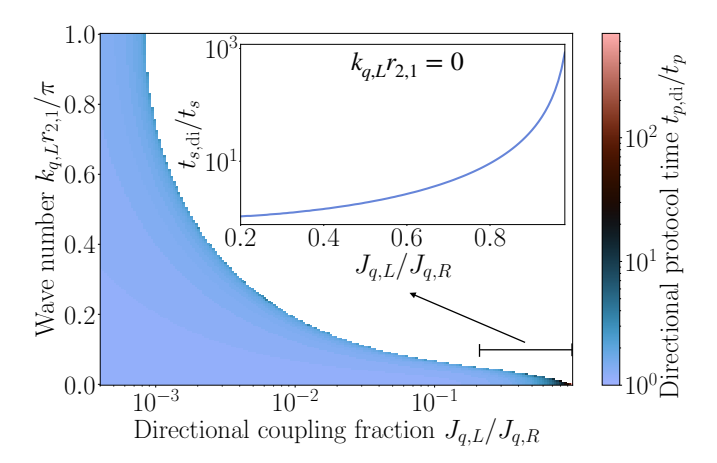


FIG. 4: Protocol time $t_{p,\mathrm{di}}$ with directional coupling normalized by the protocol time t_p with unidirectional coupling as a function of the coupling to the left $J_{q,L}$ normalized by the coupling to the right $J_{q,R}$ and as a function of the phase $k_{q,L}r_{2,1}$ normalized by π . The white coloring corresponds to the case where the fidelity threshold is not surpassed. Sufficiently small coupling $J_{q,L}$ with respect to $J_{q,R}$ still leads to convergence for all wave numbers $k_{q,L}$, while for higher $J_{q,L}$ the convergence depends on $k_{q,L}$. The inset shows $t_{s,\mathrm{di}}$ as a function of the coupling J_{-q} for $k_{q,L}r_{2,1}=0$. We use a maximal convergence time of $t_{p,\mathrm{di}}/t_p=1000$. The fidelity threshold is $F_T=0.95$, which corresponds to a protocol time $J_qt_p=73$ with $\zeta=0.27$ (see Fig. 3(a)).

A. Mediation by chiral magnons

In this subsection we discuss the interaction of a spin qubit with chiral magnons. Due to this chirality, the polarization of the magnons depends on their propagation direction. We show that the coupling constant of the qubits to the magnons depends on the magnon polarization, giving rise to a selection rule with respect to the magnon propagation direction, which leads to a unidirectional coupling.

The magnetic dipole moment $\hat{\boldsymbol{\mu}}_s = -\gamma_s \hat{\boldsymbol{S}}$ of the spin at position \boldsymbol{r}_0 , where γ_s is the modulus of the gyromagnetic ration, interacts with the magnetic field $\delta \hat{\boldsymbol{H}}(\boldsymbol{r})$ due to the magnons via

$$\hat{H}_{\text{dipole}} = -\mu_0 \hat{\boldsymbol{\mu}}_s \cdot \delta \hat{\boldsymbol{H}}(\boldsymbol{r}_0), \qquad (17)$$

where μ_0 is the vacuum magnetic permeability and

$$\delta \hat{\boldsymbol{H}}(\boldsymbol{r}) = \sum_{k} \left(\delta \boldsymbol{H}_{k}(\boldsymbol{r}) \hat{m}_{k} + \delta \boldsymbol{H}_{k}^{*}(\boldsymbol{r}) \hat{m}_{k}^{\dagger} \right), \quad (18)$$

being $\delta \mathbf{H}_k(\mathbf{r})$ the field fluctuation due to magnon mode k. We limit the description to the unidirectional axis of the magnet (see Sec. II).

The Cartesian spin components can be rewritten in terms of the spin ladder operators $\hat{S}_{\pm} = \hat{S}_x \pm i\hat{S}_y$ such that $\hat{S} = (\hat{S}_+ e_- + \hat{S}_- e_+)/\sqrt{2} + \hat{S}_z e_z$, where $e_{\pm} = (e_x \pm i\hat{S}_z + e_z)$

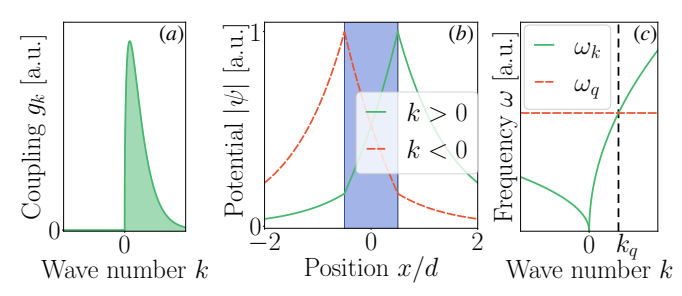


FIG. 5: Overview of the chirality and non-reciprocity leading to unidirectional spin-magnon coupling. (a) Due to chirality of the magnons and the polarization dependence of the spin-magnon coupling g_k , the coupling vanishes for one sign of the wave numbers k, but remains positive for the other, giving rise to unidirectional coupling. See Fig. 7(b) for an example. (b) Magnetic potential of a magnet exhibiting field displacement non-reciprocity (see App. F). The magnet is located between x = -d/2 and d/2, indicated in blue. Upon reversing the propagation direction $k \ge 0$, the magnetic potential shifts from one side of the magnet to the other. As a consequence, one propagation direction is more present on a specific surface than the other. (c) Sketch of the dispersion ω_k of a non-reciprocal magnon as a function of the wave number k. Due to the asymmetry in the dispersion, there is only one magnon wave number k_q which is resonant with the qubit frequency ω_q , and hence only one sign of k.

 $ie_y)/\sqrt{2}$. For spin 1/2, we express the spin raising and lowering operator in terms of the transition operators such that $\hat{S}_{\pm}^{S=1/2}=\hbar\hat{\sigma}^{\pm}$. We implement these relations and Eq. (18) in the Hamiltonian (17), on which we apply the RWA, giving

$$\hat{H}_{\text{int}}^{S=1/2} = \frac{\hbar}{\sqrt{2}} \sum_{l} (g_{k,-} \hat{\sigma}^{+} \hat{m}_{k} + g_{k,-}^{*} \hat{m}_{k}^{\dagger} \hat{\sigma}^{-}), \qquad (19)$$

where

$$g_{k,\alpha} = \gamma_s \mu_0 \delta \mathbf{H}_k(\mathbf{r}_0) \cdot \mathbf{e}_{\alpha}. \tag{20}$$

The coupling constant $g_{k,-}$ vanishes if the magnon is left polarized $(\delta H_k(r_0) \propto e_-)$, contrary to right polarization e_+ . Therefore, for chiral magnons the spin-magnon coupling is unidirectional.

In the following we will discuss an implementation with spin-1 qubits. For this case, three states $|0\rangle$, $|-\rangle$ and $|+\rangle$ are included in the description, which are eigenstates of the spin operator \hat{S}_z with eigenvalues $m_s=0$, - and +, respectively. The spin raising (lowering) operator \hat{S}_+ (\hat{S}_-) can be expressed in terms of the transition operators $\hat{\sigma}^{\alpha\beta} = |\alpha\rangle \langle \beta|$, such that $\hat{S}_{\pm}^{S=1} = \hbar \sqrt{2} (\hat{\sigma}^{\pm 0} + \hat{\sigma}^{0\mp})$ [58]. Akin to the case of the spin-1/2, we plug these relations into the interaction Hamiltonian (17) and perform the RWA. We find

$$\hat{H}_{\text{int}}^{S=1} = \hbar \sum_{k} (g_{k,+} \hat{\sigma}^{-0} + g_{k,-} \hat{\sigma}^{+0}) \hat{m}_k + \text{h.c.}$$
 (21)

If either $|-\rangle$ or $|+\rangle$ can be excluded from the dynamics of the coupled spins, then one can identify a qubit space which is spanned by the non-excluded state together with the state $|0\rangle$. Since $g_{k,+}$ or $g_{k,-}$ are non-vanishing dependent on the magnon polarization, this interaction also gives rise to a unidirectional coupling between magnons and a spin qubit with computational space $\{|0\rangle, |-\rangle\}$ or $\{|0\rangle, |+\rangle\}$.

Since the interaction Hamiltonians (19) for spin-1/2 and (21) for spin-1, after omitting the coupling of the $|0\rangle$ state to one of the triplet states $|+\rangle$ or $|-\rangle$, correspond to the Hamiltonian (3) of Sec. II and the unidirectionality condition is fulfilled, the effective qubit-qubit dynamics is described by the Liouvillian (4).

B. Mediation by non-reciprocal magnons

In the previous subsection we showed that the interaction between the spins and chiral magnons limits the coupling to only one propagation direction. Alternatively, the propagation of the magnons itself can be in certain cases unidirectional, and therefore the unidirectional coupling can be realized without resorting to chiral effects. We consider two scenarios for unidirectional propagation which can be found in magnets: field displacement and frequency non-reciprocity.

In the case of field displacement non-reciprocity, the mode profile of the magnons typically switches from one side of the magnetic structure to the other when inverting the propagation direction. The field displacement non-reciprocity was shown on a ferromagnetic slab [65, 66], where the magnon modes are referred to as Damon-Eshbach modes. In App. F we derive the magnetic potential ψ of such a ferromagnetic slab, which is shown in Fig. 5(b). Here, we see that for one propagation direction of the magnons, the potential is localized on one side of the slab, while it switches to the other side upon reversing the propagation direction. Therefore, by positioning the spins on one side of the magnet, there is only one propagation direction of the magnons present to which the spins can couple (see also Fig. 6).

Frequency non-reciprocity refers to the asymmetry in the dispersion of the magnons depending on the propagation direction (see Fig. 5(c)). There are different sources for this effect. The Dzyaloshinskii-Moriya interaction (DMI) is one of those origins [67–69, 75]. The dipolar interaction induces the non-reciprocity in curved ferromagnetic nanotubes [72, 73] and for spin waves on ferromagnetic structures [65, 66, 93, 94]. In multilayered structures, dipole-exchange interactions can give rise to asymmetries in the magnon dispersion [74, 79, 83, 84]. Frequency non-reciprocity can also give rise to unidirectional magnon-spin coupling. By tuning the frequency of the spin so that it is in a regime where only one magnon mode is present, the resonance condition $\omega_k = \omega_q$ is only satisfied for this wave number, giving rise to a unidirectional dissipative coupling (see Sec. II).

If the dispersion in the case of field displacement non-reciprocity is symmetric, then the condition $k_{q,j}r_{2,1}=2\pi n$ is automatically fulfilled for both wave numbers $k_{q,j}$ with j=L,R. Since we have shown the importance of complying with this condition in the case where the coupling is not purely unidirectional, this implies an advantage of field displacement non-reciprocity over frequency non-reciprocity.

C. Example: steady-state entanglement mediated by chiral and non-reciprocal surface magnons

Here, we apply the findings of the previous sections on a ferromagnetic thin YIG film exhibiting both chiral as well as field displacement non-reciprocal properties coupled to NV centers. The configuration is shown in Fig. 6. NV centers are a prospect platform for quantum technologies due to their relatively long coherence times [89, 95], and their integrability with other quantum systems, including photons and phonons. YIG is the magnetic material of choice in current state of the art experiments, due to its record low dissipation values for magnons [87, 96].

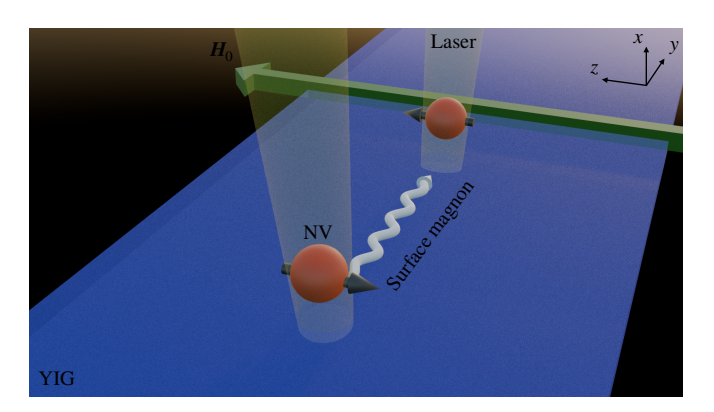


FIG. 6: Two NV centers driven at resonance by a laser are coupled unidirectionally through chiral and non-reciprocal surface magnons of a YIG slab. The propagation direction of these surface magnons is perpendicular to the external field \boldsymbol{H}_0

The ground state manifold of an NV center consists of the triplet states $|0\rangle$, $|-\rangle$ and $|+\rangle$. The $|\pm\rangle$ states are energetically separated from the $|0\rangle$ state by the zero-field splitting $\hbar D_0$. The states $|\pm\rangle$ in turn can be split by an external magnetic field H_0 , $\pm\omega_H$, with $\omega_H = \gamma_s \mu_0 H_0$. The Hamiltonian of the NV center reads

$$\hat{H}_{\text{NV}} = \sum_{\eta = \pm} \hbar \omega_{\eta} \hat{\sigma}^{\eta \eta}, \qquad (22)$$

with $\omega_{\pm} = D_0 \pm \omega_H$.

We consider a YIG film with thickness d and area $L_yL_z\gg d^2$, where $L_y\gg L_z\gg d$. We apply an in-plane external field along the z axis $\boldsymbol{H}_0=H_0\boldsymbol{e}_z$ (see Fig. 6).

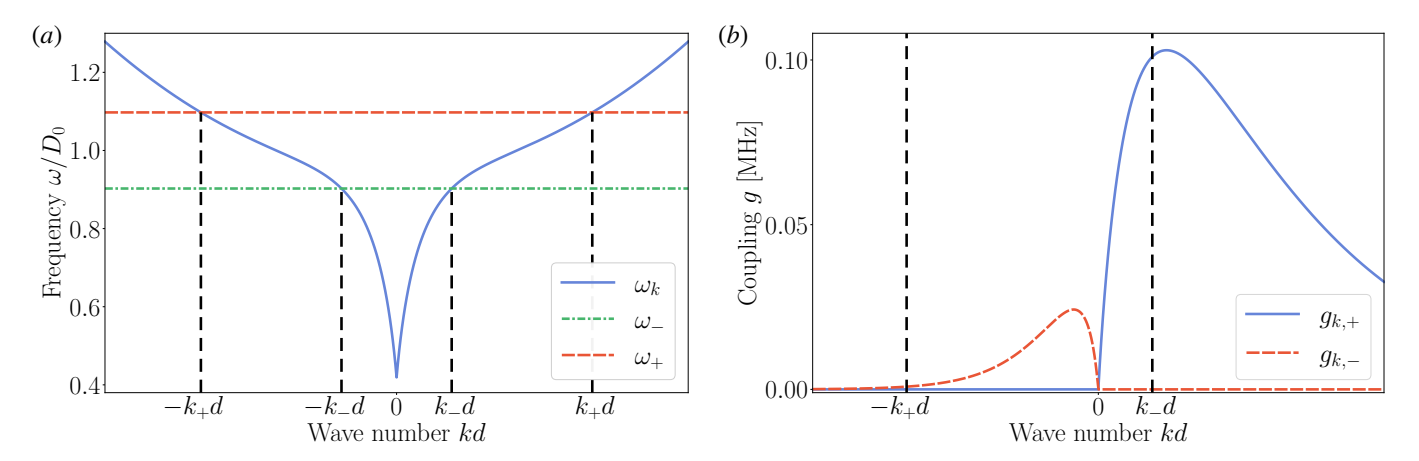


FIG. 7: (a) Frequencies ω_{\pm} of the NV states $|\pm\rangle$ and dispersion of the surface magnons ω_k along the unidirectional axis as a function of the magnon wave number k normalized by the film thickness d. For each NV frequency ω_{\pm} , there are two resonant wave numbers $\pm k_{\pm}$. (b) Coupling strengths $g_{k,\pm}$ as a function of the magnon wave number k normalized by the film thickness d, which are limited to $k \geq 0$ due to the chirality of the magnons. Thus, the coupling is non-zero at only one of the resonant wave numbers $\pm k_{\pm}$ for each frequency ω_{\pm} . The difference in amplitudes of $g_{k,\pm}$ is due to the field displacement non-reciprocity, which favors positive wave numbers (see Fig 12). The parameters chosen to obtain these figures are in Table I.

In App F we derive the frequency and the mode profiles of the surface magnons. The modes are chiral, with $\delta \boldsymbol{H}_k \propto \boldsymbol{e}_{\mp}$ for $k \geq 0$ on top of the film, and $\delta \boldsymbol{H}_k \propto \boldsymbol{e}_{\pm}$ for $k \geq 0$ on the bottom of the film, along the axis perpendicular to the in plane external field, i.e. the y axis. We neglect the higher-order magnon modes with $k_z > 0$ given that they are far detuned from the NV frequencies, $g_{n_z=1,k} \ll |\omega_{n_z=1,k} - \omega_q|$, where n_z is defined with $k_z = 2\pi n_z/L_z$. This approximation enables us to focus on the surface magnons propagating along the y axis with $k_z = 0$.

We consider two NV centers positioned on top of the YIG film along the unidirectional y axis. Under the RWA, the interaction of the NV centers with the surface magnons is given by the interaction Hamiltonian of Eq. (21) [52, 54–64]. The magnon frequency ω_k together with the frequencies ω_{\pm} of the qubit are displayed in Fig. 7(a). There are two magnon wave numbers $\pm k_{-}$ which are resonant with the NV frequency $\omega_{-} = \omega_{\pm k_{-}}$. This also holds for $\omega_{+} = \omega_{\pm k_{+}}$, as one can see in Fig. 7(a). Note that the magnon wave number k_{+} is significantly higher than k_{-} , as one can see in Fig. 7(a), due to the monotonic shape of the magnon dispersion and the fact that ω_{+} is larger than ω_{-} .

Due to chirality, the NV-magnon coupling is unidirectional (see Sec. IV A), where the $|0\rangle \leftrightarrow |-\rangle$ transition of the NV is limited to coupling with e_- polarized magnons propagating to the right (with coupling constant $g_{k,+}$), while the transition $|0\rangle \leftrightarrow |+\rangle$ is limited to left-propagating magnons with polarization e_+ ($g_{k,-}$). Due to the field displacement non-reciprocity, which favors right-propagating magnons, the coupling $g_{k,-}$ is suppressed with respect to $g_{-k,+}$ (see Fig. 7(b)). This field displacement non-reciprocity together with the

higher resonant wave number k_+ compared to k_- gives rise to $g_{-k_+,-}/g_{k_-,+} \approx 10^{-2}$. Therefore, we can neglect the $|0\rangle \leftrightarrow |+\rangle$ with respect to the $|0\rangle \leftrightarrow |-\rangle$ to a good approximation [58]. Thus, we identify $|0\rangle$ and $|-\rangle$ as the computational basis states. From now on, we refer to the frequency ω_- as the qubit frequency ω_q . Since the unidirectionality condition is fulfilled and the dynamics of the NV center can be truncated to two states, we obtain the Liouvillian given in Eq. (4).

Besides the instantaneous coupling conditions $|\delta_q|, J_q, \Omega \ll v_{k_q}/r_{2,1}$ (see Eq. (7)), the distance between the coupled qubits $r_{2,1}$ cannot exceed the coherence length of the magnons. For YIG films, the coherence length l_m is limited by the lifetime of the magnons $\tau_m.$ Using $l_m=v_{k_q}\tau_m$ and $\tau_m=1\,\mathrm{\mu s}$ [87] gives rise to $l_m=3\,\mathrm{mm}.$ We check whether this coherence length is the limiting factor in the qubit distance $r_{2,1}$. Using the parameters given in Table I, we determine $J_q=190\,{\rm Hz}.$ We note that there is no dependence of J_q on L_y . We find $J_q/(v_{k_q}/l_m)=10^{-3}.$ Thus, the magnon coherence length is indeed the limiting factor. As a consequence, given that the qubit decoherence plays no role, the protocol can allow entangled spins with a distance exceeding microns, with the minimal qubit distance equaling $2\pi/k_q = 1.3\,\mu\text{m}$. This qubit distance is also such that the direct interaction between the NV centers is negligible [97]. For completeness, we note that $\tau_m / \tau_{\delta,\Omega} = 10^{-3}$.

To test the applicability of the protocol, we put the value of the dissipative coupling strength J_q into context using the benchmark for the decoherence. Since the dephasing time is typically the critical factor for NV centers [86], we focus on this quantity in our discussion. A minimal fidelity of 0.95 requires a dephasing

time $T_{\phi}=280/J_{q}$ according to Fig. 3(c). For the determined coupling strength, this corresponds to $T_{\phi}=1.5\,\mathrm{s}$. Since the current dephasing times are in the order of seconds [89], this is the bottleneck of the protocol. We note that the protocol can be further combined with dynamical decoupling protocols [88, 98].

Lastly, we recall that to arrive at the Liouvillian in Eq. (4), we assumed that the magnon sector of the initial state is in the vacuum state, that is, a state with zero-magnon occupation. Since the protocol builds on the resonance of spins and magnons, the magnon vacuum requires a temperature $\mathcal{T} \ll \hbar \omega_q/k_B$. The frequencies of spin qubits are typically in the range $1-30\,\mathrm{GHz}$ [86, 99], corresponding to a temperature range $8-230\,\mathrm{mK}$, which are routinely achievable in commercially available dilution fridges [24, 37, 38, 40, 100]. For a NV-center qubit specifically, the qubit frequency lies in the regime of the zero-field splitting $D_0=18\,\mathrm{GHz}$ [86], corresponding to a temperature $\mathcal{T}=138\,\mathrm{mK}$.

V. CONCLUSIONS

We demonstrated that unidirectional coupling between magnons and spin qubits can be realized with magnets displaying field displacement or frequency non-reciprocity, chirality, or a combination of these. We showed that under the Born-Markov approximation the spin qubits are unidirectionally and dissipatively coupled. Exploiting this coupling, we proposed a protocol which evolves the product state $|00\rangle$ of two qubits into a maximally entangled Bell state. Since this state is the steady state of the system, any initial qubit state converges to this entangled state, given that the distance r between the two qubits satisfies $k_q r = 2\pi n$, where k_q is the resonant magnon wave number and n is an integer. We discussed the application of the protocol on both chiral and non-reciprocal magnets.

We proposed and benchmarked the protocol for a hybrid system consisting of NV centers coupled via the surface magnons of a YIG film. Due to the high coherence length of magnons in YIG, steady-state entanglement can be achieved for qubits separated by a distance r surpassing microns. We showed that the dephasing time T_{ϕ} of the NV centers is the limiting factor to achieve this entanglement in this hybrid system, requiring $T_{\phi} = 1.5 \, \text{s}$. The protocol requires to be performed at cryogenic temperatures to suppress the thermal occupation of the magnons.

Stronger coupling between spin qubits and magnons helps to speed up the protocol, limiting the deteriorating effects of the intrinsic decoherence of the qubits. Recently, the strong coupling of an antiferromagnet (AFM) to electron spins has been demonstrated, where the electron spins are either doped directly into the AFM lattice [101] or hosted in a separate magnetic layer interfaced with the AFM [102]. Whereas the spinmagnon coupling of the rare-earth-doped AFM lacks non-reciprocity or chirality [101], such properties can be

achieved by, e.g., magnetization grading [76] or by forming multilayered structures [80–84], providing an alternative promising platform for magnon-mediated steady-state entanglement. Alternatively, Ref. [102] demonstrated that the AFM magnons can be tuned in-situ between linear and chiral modes, making this hybrid system suitable for the protocol and implying the possibility of combining it with bidirectional protocols.

Natural extensions to the protocol could involve harnessing the two-dimensional chiral coupling between emitters above a magnetic film. It has been shown [58] that for the right spatial configuration an emitter can couple chirally to emitters along not one but two welldefined directions, in analogy to a qubit placed at the intersection of two chiral waveguides. This could enable more complex physics and protocols such as e.g. the preparation of an entangled state between two qubits lying each on one of the effective "waveguides" by spontaneous decay of the original emitter. A second potential extension would be to explore the transition between coherent and dissipative coupling between emitters, either in purely magnonic or in hybrid magnonicmicrowave platforms. Since the nature of the coupling depends on the wavelength of the magnons at the qubit energy, it should be possible to explore the transition between these two regimes by tuning the magnon dispersion relation. Lastly, the dissipative generation of singlet states of well separated NV centers can find applications in quantum sensing [103], gradiometry and distributed quantum computing applications [104]. As the total evolution of our open quantum system is governed by the non-Hermitian operator $H_Q + H_{\text{eff}}$, exceptional points (EPs) can be formed as shown in Fig. 8. The EP here is formed by the coalescence of two modes with varying singlet fraction (Eq. (B3)) and coalesce at R=4 (see Appendix B). The system's spectral response is maximally nonlinear in the vicinity of the EP, which could lead to higher sensitivity quantum sensing applications [105, 106]. Exploring these regimes is left for future work.

ACKNOWLEDGMENTS

M.D., M.C. D.B.R.D., and S.V.K. acknowledge financial support by the Federal Ministry of Research, Technology and Space (BMFTR) project QECHQS (Grant No. 16KIS1590K). C.G.B. acknowledges the Austrian Science Fund FWF for the support with the project PAT-1177623 "Nanophotonics-inspired quantum magnonics".

Appendix A: Effective qubit-qubit dynamics

In this Appendix we use the Born-Markov approximation to trace out the magnon bath and derive the equation of motion of unidirectionally coupled spin qubits.

The Heisenberg equation of motion for the magnon annihilation operator \hat{m} using the Hamiltonians (1) and

(3) is given by

$$\frac{\mathrm{d}}{\mathrm{d}t}\hat{m}_{\mathbf{k}} = -i\delta_{\mathbf{k}}\hat{m}_{\mathbf{k}} - i\sum_{j} g_{j,\mathbf{k}}^{*}\hat{\sigma}_{j}^{-}.$$
 (A1)

This equation is evaluated in the rotating frame of the drive, where $\delta_{\mathbf{k}} = \omega_{\mathbf{k}} - \omega_d$ is the detuning of the magnons. We solve the equation of motion (EOM) for the magnon annihilation operator formally to obtain

$$\hat{m}_{\mathbf{k}}(t) = \hat{m}_{\mathbf{k}}(0)e^{-i\delta_{\mathbf{k}}t} - i\sum_{j} g_{j,\mathbf{k}}^{*} \int_{0}^{t} d\tilde{t}\hat{\sigma}_{j}^{-}(\tilde{t})e^{-i\delta_{\mathbf{k}}(t-\tilde{t})}.$$
(A2)

Plugging this relation into the EOM for a generic qubit operator \hat{a} gives (all operators evaluated at time t)

$$\frac{\mathrm{d}}{\mathrm{d}t}\hat{a} = \frac{i}{\hbar} \left(\left[\hat{H}_Q, \hat{a} \right] + \sum_i \left[\hat{\sigma}_i^+, \hat{a} \right] (\hat{\mathcal{N}}_i - i\hat{\mathcal{B}}_i) \right. \\
\left. + (\hat{\mathcal{N}}_i^{\dagger} + i\hat{\mathcal{B}}_i^{\dagger}) \left[\hat{\sigma}_i^-, \hat{a} \right] \right), \tag{A3}$$

where we identified a noise term

$$\hat{\mathcal{N}}_i = \sum_{\mathbf{k}} \hbar g_{i,\mathbf{k}} \hat{m}_{\mathbf{k}}(0) e^{-i\delta_{\mathbf{k}}t}$$
 (A4)

and a back-action term

$$\hat{\mathcal{B}}_{i} = \sum_{j,k} \hbar g_{i,k} g_{j,k}^{*} \int_{0}^{t} d\tilde{t} \hat{\sigma}_{j}^{-}(\tilde{t}) e^{i\delta_{k}(t-\tilde{t})}.$$
 (A5)

We make the Markov approximation $\hat{\sigma}_j^-(\tilde{t}) \approx \hat{\sigma}_j^-(t)$, which is valid for $\tau_m \ll \tau_q$, $\tau_{\delta,\Omega}$, where τ_m and τ_q are the correlation time of the magnon bath and of the spin qubit, respectively, and $\tau_{\delta,\Omega} = 2/\sqrt{\delta^2 + 4\Omega^2}$ is the time constant associated with the driving of the qubit. This gives rise to $\hat{\mathcal{B}}_i = \sum_j \hbar J_{i,j} \hat{\sigma}_j^-(t)$, where

$$J_{i,j} = \sum_{\mathbf{k}} \hbar g_{i,\mathbf{k}} g_{j,\mathbf{k}}^* \int_0^\infty d\tilde{t} e^{-i\delta_{\mathbf{k}}(t-\tilde{t})}.$$
 (A6)

We return to the EOM of Eq. (A3) and use $\operatorname{Tr}\left\{\frac{\mathrm{d}\hat{a}}{\mathrm{d}t}\hat{\rho}_{\mathrm{tot}}^{H}\right\} = \operatorname{Tr}\left\{\hat{a}\frac{\partial\hat{\rho}_{\mathrm{tot}}}{\partial t}\right\}$ to switch from the Heisenberg picture to the Schrödinger picture [2]. Here, $\hat{\rho}_{\mathrm{tot}}^{H}$ is the density operator for the complete system (so both qubits as magnons) in the Heisenberg picture. We employ the Born approximation, i.e. we consider that the qubit state is separable from the magnon state, which is assumed to be in the thermal state, i.e. $\hat{\rho}_{\mathrm{tot}}^{H} = \hat{\rho}_{Q}^{H} \otimes \hat{\rho}_{\mathrm{th}}^{H}$. Therefore, the trace over the magnonic part of the noise terms $\hat{\mathcal{N}}_{i}^{(\dagger)}$ will vanish. This leads to

$$\frac{\partial \hat{\rho}}{\partial t} = -\frac{i}{\hbar} \left[\hat{H}_Q, \hat{\rho} \right] - \sum_{i,j} J_{i,j} \left[\hat{\sigma}_i^+, \hat{\sigma}_j^- \hat{\rho} \right] + J_{i,j}^* \left[\hat{\rho} \hat{\sigma}_j^+, \hat{\sigma}_i^- \right],$$
(A7)

where $\hat{\rho} = \text{Tr}_Q \{\hat{\rho}_{\text{tot}}\}$. To arrive at this equation, we assumed that the interaction between qubit i and j is

instantaneous. This requires $|\delta_q|$, Ω , $|J_{i,j}| \ll v_m/r_{i,j}$, where v_m is the group velocity of the magnons along the axis where the qubits are positioned.

This master equation does not explicitly state the unidirectional coupling between the qubits. This comes into play when evaluating the coupling $J_{i,j}$. The time integral of $J_{i,j}$ in Eq. (A6) gives rise to [107]

$$\int_0^\infty d\tilde{t} e^{-i(\omega_{\mathbf{k}} - \omega_q)(t - \tilde{t})} = \pi \delta \left(\omega_{\mathbf{k}} - \omega_q\right) - i\mathcal{P}\left(\frac{1}{\omega_{\mathbf{k}} - \omega_q}\right). \tag{A8}$$

Here, we used $\omega_d = \omega_q$. We rewrite the coupling to $J_{i,j} = \gamma_{i,j}/2 + i\Omega_{i,j}$, where

$$\gamma_{i,j} = 2\pi \sum_{\mathbf{k}} g_{i,\mathbf{k}} g_{j,\mathbf{k}}^* \delta\left(\omega_{\mathbf{k}} - \omega_q\right)$$
 (A9)

and

$$\Omega_{i,j} = -\sum_{\mathbf{k}} g_{i,\mathbf{k}} g_{j,\mathbf{k}}^* \mathcal{P} \left(\frac{1}{\omega_{\mathbf{k}} - \omega_q} \right). \tag{A10}$$

If one would plug this relation for $J_{i,j}$ into the EOM of Eq. (A7), one would identify $\gamma_{i,j}$ as a dissipative and $\Omega_{i,j}$ as a coherent coupling.

Now, we focus on the unidirectional axis. We find a dissipative coupling

$$\gamma_{i,j} = \frac{2\pi \mathcal{D}(k_q)|g_{k_q}|^2}{|v_{k_q}|} e^{ik_q r_{i,j}}$$
 (A11)

where we used $g_{i,k} = g_k \exp(ikr_i)$. Also, we introduced the wave number k_q which corresponds to a magnon frequency equal to the qubit frequency $\omega_{k_q} = \omega_q$, the density of states $\mathcal{D}(k)$ and the group velocity $v_k = \partial \omega_k / \partial k$. Note that in reciprocal and symmetric ($\omega_k = \omega_{-k}$) systems, the dissipative coupling in Eq. (A11) would have another term involving $-k_q$. However, due to $g_{-k_q} = 0$ (chiral and field displacement non-reciprocity) or simply the lack of resonance for a wave number other than k_q (frequency non-reciprocity), there is only the term given rise to the resonance condition $\omega_{k_q} = \omega_q$. For the coherent coupling one finds [108]

$$\Omega_{i,j} = -\frac{i\pi \mathcal{D}(k_q)|g_{k_q}|^2}{v_{k_q}} e^{ik_q r_{i,j}} \operatorname{sgn}(r_{i,j}).$$
 (A12)

This yields for $v_{k_q} > 0$

$$J_{i,j} = \frac{J_q}{2} e^{ik_q r_{i,j}} (1 + \operatorname{sgn}(r_{i,j})),$$
 (A13)

where $J_q = 2\pi \mathcal{D}(k_q)|g_{k_q}|^2/|v_{k_q}|$. This results in

$$J_{i,i} = \frac{J_q}{2}, \quad J_{i>j} = J_q e^{ik_q r_{i,j}}, \quad J_{i< j} = 0.$$
 (A14)

With these relations we find that the EOM of Eq. (A7) can be rewritten such that one obtains the Liouvillian of

Eq. (4), which shows a unidirectional coupling towards the right $(r_i > r_j)$.

For $v_{k_q} < 0$ one finds

$$J_{i,j} = \frac{J_q}{2} e^{ik_q r_{i,j}} \left(1 - \operatorname{sgn}(r_{i,j}) \right), \tag{A15}$$

which results in a unidirectional coupling towards the left $(r_i < r_j)$.

Appendix B: Eigenstates of the Hamiltonian $\hat{H}_Q + \hat{H}_{\mathrm{eff}}$

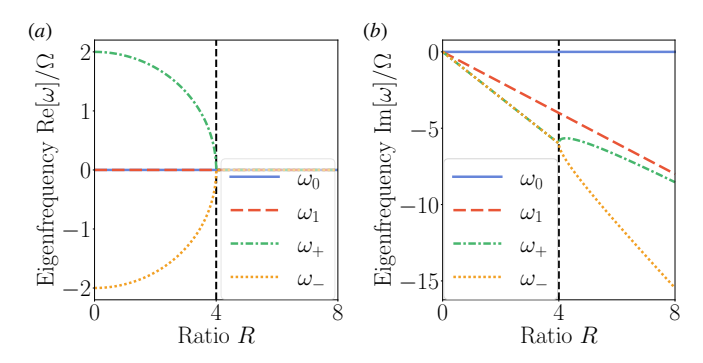


FIG. 8: (a) Real part and (b) imaginary part of the eigenfrequencies of $\hat{H}_Q + \hat{H}_{\text{eff}}$ as function of $R = J_q/(2\Omega)$ for two qubits and $\delta = 0$ and $k_q r_{2,1} = 2\pi n$. The exceptional point of the frequencies ω_{\pm} at R = 4 is indicated with a vertical dashed line.

To obtain the eigenstates of the Hamiltonian $\hat{H}_Q + \hat{H}_{\text{eff}}$ for two resonantly driven qubits $\delta = 0$ and positioned such that $k_q r_{2,1} = 2\pi n$, we solve the equation $(\hat{H}_Q + \hat{H}_{\text{eff}}) |\psi_i\rangle = \hbar \omega_i |\psi_i\rangle$. Since the dimension of the Hilbert space is four, we obtain four eigenstates. The first eigenfrequency equals $\omega_0 = 0$ with eigenstate

$$|\psi_0\rangle \propto iR |00\rangle - |01\rangle + |10\rangle,$$
 (B1)

with $R = J_q/(2\Omega) > 0$. The second eigenfrequency equals $\omega_1 = -iJ_q/2$ with eigenstate

$$|\psi_1\rangle \propto |00\rangle - iR|01\rangle - |11\rangle$$
, (B2)

while the third and fourth eigenfrequencies equal $\omega_{\pm} = (-3iR/2 \pm \nu)\Omega$ with eigenstates

$$|\psi_{\pm}\rangle \propto \left(2 \pm i\nu R - \frac{1}{2}R^2\right)|00\rangle$$

$$+ \left(\frac{1}{2}iR(R^2 - 1) \pm \nu(R^2 + 1)\right)|01\rangle \qquad (B3)$$

$$+ \left(\frac{3}{2}iR \pm \nu\right)|10\rangle + \left(2 + R^2\right)|11\rangle.$$

Here, $\nu = \sqrt{(4-R)(4+R)}/2$. For R=4 one finds $\nu = 0$ and hence $\omega_+ = \omega_-$, while for all other R one

finds $\omega_+ \neq \omega_-$. Also, one finds that the eigenstates $|\psi_{\pm}\rangle$ coalesce for R=4, since $\langle \psi_- | \psi_+ \rangle = 1$. Therefore, R=4 is an exceptional point.

In Fig. 8(a) we display the real and in Fig. 8(b) the imaginary parts of these eigenvalues. At the exceptional point R=4, we see indeed that the eigenvalues ω_{\pm} are equal to each other.

Application of the Lindblad operator given in Eq. (7) on the eigenstate $|\psi_0\rangle$ of Eq. (B1) gives $\hat{L} |\psi_0\rangle = 0$. Since $|\psi_0\rangle$ is an eigenstate of $\hat{H}_Q + \hat{H}_{\text{eff}}$ and is in the null space of the Lindblad operator, this state is a dark state of the Liouvillian of Eq. (4). Normalization of $|\psi_0\rangle$ gives rise to the state given in Eq. (8).

Appendix C: Transient time versus protocol time

We examine the time required for the system to reach the steady state, i.e. the transient time t_s . We quantify this by computing the overlap of the state of the system $\hat{\rho}(t)$ at time t with the steady state $|\psi_s\rangle$, leading to $\sqrt{\langle \psi_s | \hat{\rho}(t) | \psi_s \rangle}$. The state $\hat{\rho}(t)$ is found by the master equation given by the Liouvillian in Eq. (4), using the initial state $\hat{\rho}_{00}$. We do this comparison for three cases, which are are the minimal protocol times which we found in Fig. 3(a). These protocol times are $J_q t_{p,1} = 73$, $J_q t_{p,2} = 134$ and $J_q t_{p,3} = 503$, with the fidelity thresholds $F_{T,1} = 0.95$, $F_{T,2} = 0.97$ and $F_{T,3} = 0.99$. These values correspond to $\zeta_1 = 0.27$, $\zeta_2 = 0.22$, and $\zeta_3 = 0.13$, respectively. Note that $\zeta_1 > \zeta_2 > \zeta_3$. As one can see in Fig. 9, a lower ζ corresponds to more time t required to reach a steady-state overlap ~ 1 , giving rise to a higher transient time t_s .

We compare the transient time t_s with the protocol time t_p we find in Sec. III, i.e. the time needed for the system to be equal to the entangled state $|\psi_{-}\rangle$ within a specific fidelity threshold F_T . Also, note that at the dashed lines, which are the protocol times $t_{p,i}$ for a specific ζ_i , that the system has not fully converged yet towards the steady state, since the steady-state overlap is not equal to 1 yet.

Appendix D: Variation of the parameter ζ

Here, we analyze the consequences of a variation in $\zeta = J_q/(2\sqrt{2}\Omega)$. In the optimization of the protocol time t_p versus ζ for a given fidelity threshold F_T , we find a ζ_{\min} which minimizes the protocol time, giving $t_{p,\min}$, see Fig. 3(b). Here, we see that the protocol time is relatively flat around the minimum, indicating a wide range of ζ with a similar protocol time. To quantify this, we examine the variation in the protocol t_p for a given (relative) error in ζ with respect to the optimal ζ_{\min} , resulting in Fig. 10(a). Here, one sees that the allowed variation of ζ compared to the threshold value ζ_T depends on the set fidelity F_T . A higher fidelity F_T comes at the cost of a lower allowed variation in ζ with respect to the threshold

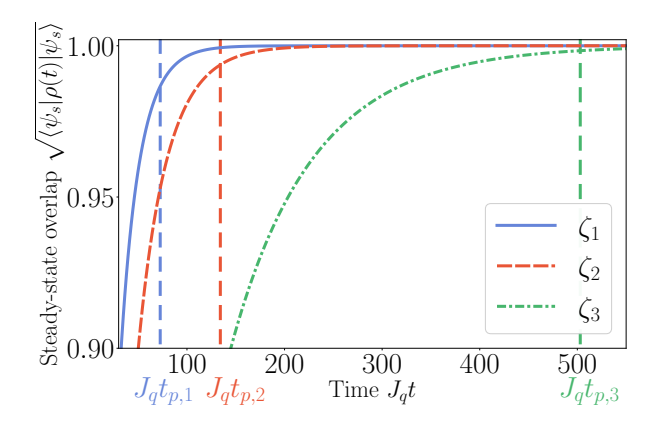


FIG. 9: Steady-state overlap $\sqrt{\langle \psi_s | \hat{\rho}(t) | \psi_s \rangle}$ of the system $\hat{\rho}(t)$ at the time t normalized by the coupling constant J_q for different $\zeta_1 > \zeta_2 > \zeta_3$. A higher steady-state overlap requires more time t. Also, a lower ζ corresponds to less time needed to reach the steady state and hence also to a lower transient time t_s . The vertical dashed lines correspond to the minimal protocol times $t_{p,i}$ found in Fig. 3(a) for a specific ζ_i .

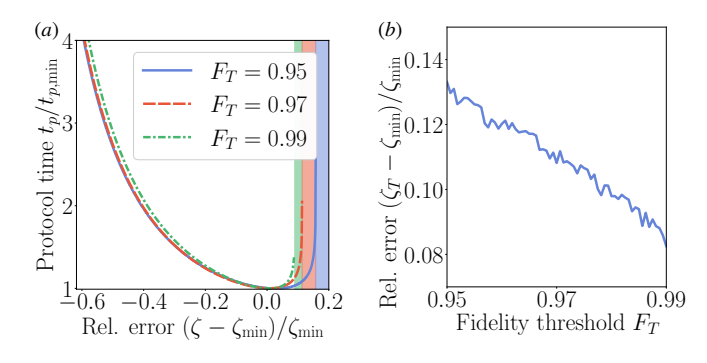


FIG. 10: (a) Protocol time t_p normalized by the minimal time $t_{p,\text{min}}$ as a function of the relative error of ζ with respect to the optimal ζ_{min} which minimizes the protocol time. The threshold values ζ_T are indicated with a vertical line, which correspond to different fidelities F_T (see Eq. (10)). (b) Relative error of the threshold value ζ_T with respect to the optimal ζ_{min} as a function of the fidelity threshold F_T .

value ζ_T . The threshold value ζ_T is relevant, because an error such that ζ surpasses the threshold ζ_T prohibits the protocol to converge. Therefore, we analyze this variation of ζ_T with respect to the optimal value ζ_{\min} as a function of the fidelity threshold in Fig. 10(b), setting an upper bound on the allowed error in ζ . Since the relative error $(\zeta_T - \zeta_{\min})/\zeta_{\min}$ decreases for increasing fidelity F_T , we find once more that a higher fidelity requires a more precise configuration.

Appendix E: Variation of the qubit distance $r_{2,1}$

In this Appendix, we test the degree of variation in the qubit distance condition $k_q r_{2,1} = 2\pi n$ the protocol allows. As an example, we take $\zeta = 0.27$, $J_q t_p = 73$, which correspond to $F_T = 0.95$ (see Sec. C). First, we vary $k_q r_{2,1}$ and compute the fidelity $F(t_p)$, where F(t) is the fidelity of the state $\hat{\rho}(t)$ of the system at time t with the entangled state $|\psi_-\rangle$ (see Eq. 9). This results in Fig. 11(a). The fidelity $F(t_p)$ decreases more, The further the phase $k_q r_{2,1}$ varies from $2\pi n$, the more the fidelity $F(t_p)$ decreases. At $k_q r_{2,1} = \pi/2$ the fidelity reaches a minimum $F(t_p) = 1/2$, where the steady state of the system corresponds to the maximally mixed state $(\hat{\rho}_{00} + \hat{\rho}_{01} + \hat{\rho}_{10} + \hat{\rho}_{11})/4$ with $\hat{\rho}_{ij} = |ij\rangle \langle ij|$.

Since the time propagation of the system is stopped at a fixed time t_p in the discussion above, where $k_q r_{2,1} = 0$ reaches the set fidelity threshold, the system does not reach this threshold for $k_q r_{2,1} \neq 0$. To investigate whether the system reaches the fidelity threshold at all, we fix the fidelity threshold to $F_T = 0.95$ as above and compute the time needed to surpass this threshold while varying the phase $k_q r_{2,1} \neq 0$, giving rise to $t_{p,\varphi}$ and Fig. 11(b). Here, we see that for $|k_q r_{2,1}| > 0.015 \times \pi$ the protocol does not converge, since the overlap of the steady state with the entangled state is insufficient. This imposes an upper bound on the admitted variation on $k_q r_{2,1}$.

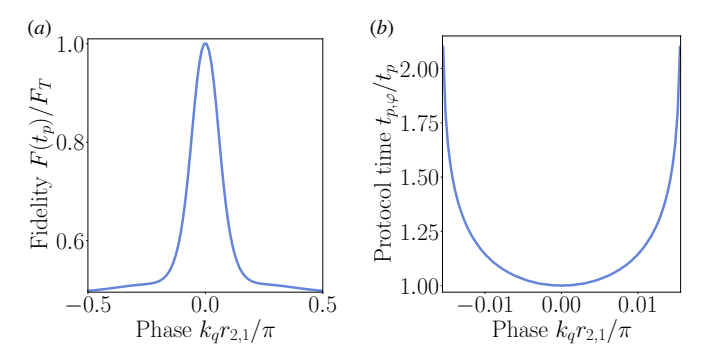


FIG. 11: (a) Fidelity $F(t_p)$ evaluated at the protocol time t_p , which is normalized by the fidelity threshold F_T (see text) as a function of the phase $k_q r_{2,1}$. (b) Protocol time $t_{p,\varphi}$ normalized by the protocol time t_p as a function of the phase $k_q r_{2,1}$

Appendix F: Chiral magnon surface modes

In this Appendix, we derive the magnon-spin coupling for a ferromagnetic film of thickness d placed in a uniform, tangential magnetic field. We focus on the Damon-Eshbach configuration [65], in which spin waves propagate perpendicular to the field direction. In this case, the boundary condition for the normal component of the

TABLE I: Summary of the parameters used to estimate the NV-magnon coupling $g_{k,\pm}$ and the dissipative coupling J_q .

Parameter	Value
NV zero-field splitting	$D_0 = 2\pi \times 2.877 \mathrm{GHz}$
Gyromagnetic ratio	$\gamma_s = 1.76 \times 10^{11} \mathrm{T}^{-1} \mathrm{s}^{-1}$
YIG film thickness	$d = 200\mathrm{nm}$
YIG film length	$L_y = 10 \mu \mathrm{m}$
YIG film width	$L_z = 1 \mu \mathrm{m}$
YIG exchange stiffness	$D_{\rm ex} = 3.086 \times 10^{-16} \mathrm{m}^2$
YIG saturation magnetization	$M_s = 1.39 \times 10^5 \mathrm{Am}^{-1}$
YIG surface to NV distance	$d_{ m NV} = d/2$
External field amplitude	$\mu_0 H_0 = 10^{-2} \mathrm{T}$

magnetic flux density \boldsymbol{B} requires

$$(1 + \chi_{\rm d}) \left[\frac{\partial \psi^i}{\partial x} - i \chi_{\rm a} \frac{\partial \psi^i}{\partial y} \right] \bigg|_{x = \pm d/2} = \left. \frac{\partial \psi^e}{\partial x} \right|_{x = \pm d/2},$$
(F1)

and the continuity of the tangential component of the magnetic field \boldsymbol{H} implies

$$\psi^i\big|_{x=\pm d/2} = \psi^e\big|_{x=\pm d/2} + \text{const.}$$
 (F2)

The additive constant in Eq. (F2) can be omitted. In Eq. (F1), χ_d and χ_a denote the diagonal and antidiagonal components of the Polder susceptibility tensor [109]. These components are given by

$$\chi_{\rm d} = \frac{\omega_{\rm M} \left(\omega_{\rm H} + \omega_{\rm M} k_y^2 D_{\rm ex}\right)}{\left(\omega_{\rm H} + \omega_{\rm M} k_y^2 D_{\rm ex}\right)^2 - \omega_k^2},$$

$$\chi_{\rm a} = \frac{\omega_k \omega_{\rm M}}{\left(\omega_{\rm H} + \omega_{\rm M} k_y^2 D_{\rm ex}\right)^2 - \omega_k^2},$$
(F4)

$$\chi_{\rm a} = \frac{\omega_k \omega_{\rm M}}{\left(\omega_{\rm H} + \omega_{\rm M} k_n^2 D_{\rm ex}\right)^2 - \omega_k^2},\tag{F4}$$

where $\omega_{\rm M} = \gamma_s \mu_0 M_s$. The internal and external magnetic potentials, ψ^i and ψ^e , satisfy Walker's and Laplace's equations, respectively:

$$(1 + \chi_{\rm d}) \left(\frac{\partial^2 \psi^i}{\partial x^2} + \frac{\partial^2 \psi^i}{\partial y^2} \right) + \frac{\partial^2 \psi^i}{\partial z^2} = 0, \quad (F5)$$

$$\frac{\partial^2 \psi^e}{\partial x^2} + \frac{\partial^2 \psi^e}{\partial y^2} + \frac{\partial^2 \psi^e}{\partial z^2} = 0.$$
 (F6)

The corresponding solutions are assumed as

$$\psi^{i} = \left(A\sin(k_x^{i}x) + B\cos(k_x^{i}x)\right)e^{ik_yy}\cos(k_zz) \quad (F7)$$

in the ferromagnet $-d/2 \le x \le d/2$,

$$\psi^e = De^{k_x^e x} e^{ik_y y} \cos(k_z z) \tag{F8}$$

below the ferromagnet x < -d/2, and

$$\psi^e = Ce^{-k_x^e x} e^{ik_y y} \cos(k_z z) \tag{F9}$$

above the ferromagnet x > d/2. Substituting into Eqs. (F5) and (F6) yields the characteristics relations:

$$(1 + \chi_{\rm d}) \left[(k_x^i)^2 + k_y^2 \right] + k_z^2 = 0,$$
 (F10)

$$-(k_x^e)^2 + k_y^2 + k_z^2 = 0. (F11)$$

We assume that the ferromagnet boundaries discretize the wave numbers along the z axis as $k_z = 2\pi n_z/L_z$, where $n_z \in \mathbb{Z}$. Two types of magnon modes arise: volume and surface. The volume modes are characterized by real wave numbers, whereas the surface mode corresponds to an imaginary k_x^i and real k_y, k_z in the chosen geometry.

We focus on the surface mode with $k_z = 0$, assuming that the higher-order modes with $k_z > 0$ are far detuned from the qubit frequency,

$$g_{n_z=1,k_y} \ll |\omega_{n_z=1,k_y} - \omega_q|, \tag{F12}$$

This approximation allows us to restrict the analysis to magnons propagating along the y axis with $k_z = 0$. From Eqs. (F10, F11) it then follows that

$$(k_x^i)^2 = -k_y^2, (F13)$$

$$(k_x^e)^2 = k_y^2, (F14)$$

which implies that k_x^i is purely imaginary and continuous. We choose

$$k_x^i = ik_y, (F15)$$

$$k_x^e = |k_y|. (F16)$$

With this choice, the case $k_y > 0$ corresponds to a potential distribution that attains its maximum at the upper surface x = d/2 (see also Fig. 5(b)).

In addition, we find the dispersion equation that describes the magnon frequency

$$\omega_k^2 = \omega_{\rm H}' \left(\omega_{\rm H}' + \omega_{\rm M} \right) + \frac{\omega_{\rm M}^2}{2} \left(\frac{1}{2} - \frac{e^{-2|k_y|d}}{2} \right), \quad (F17)$$

where $\omega_{\rm H}' = \omega_{\rm H} + \omega_{\rm M} D_{\rm ex} k_y^2$.

Substituting the solutions into the boundary conditions Eqs. (F1, F2) yields

$$-iA\sinh\left(\frac{k_yd}{2}\right) + B\cosh\left(\frac{k_yd}{2}\right) - De^{-\frac{1}{2}|k_y|d} = 0,$$

$$iA\sinh\left(\frac{k_yd}{2}\right) + B\cosh\left(\frac{k_yd}{2}\right) - Ce^{-\frac{1}{2}|k_y|d} = 0,$$

$$[iAk_y(1+\chi_{\rm d}) + Bk_y\chi_{\rm a}]\cosh\left(\frac{k_yd}{2}\right) - [Bk_y(1+\chi_{\rm d}) + iAk_y\chi_{\rm a}]\sinh\left(\frac{k_yd}{2}\right) - D|k_y|e^{-\frac{1}{2}|k_y|d} = 0,$$

$$[iAk_y(1+\chi_{\rm d}) + Bk_y\chi_{\rm a}]\cosh\left(\frac{k_yd}{2}\right) + [Bk_y(1+\chi_{\rm d}) + iAk_y\chi_{\rm a}]\sinh\left(\frac{k_yd}{2}\right) + C|k_y|e^{-\frac{1}{2}|k_y|d} = 0,$$

$$[iAk_y(1+\chi_{\rm d}) + Bk_y\chi_{\rm a}]\cosh\left(\frac{k_yd}{2}\right) + [Bk_y(1+\chi_{\rm d}) + iAk_y\chi_{\rm a}]\sinh\left(\frac{k_yd}{2}\right) + C|k_y|e^{-\frac{1}{2}|k_y|d} = 0,$$

where we employed Eqs. (F15) and (F16).

Solving the Eqs. (F18) yields

$$B = iA \frac{\tanh\left(\frac{k_y d}{2}\right) (|k_y| - \chi_a k_y) + (1 + \chi_d) k_y}{-\chi_a k_y + |k_y| + (1 + \chi_d) k_y \tanh\left(\frac{k_y d}{2}\right)}$$
(F19)

$$C = iA \frac{(|k_y| - \chi_a k_y) \sinh(k_y d) + (1 + \chi_d) k_y \cosh(k_y d)}{(|k_y| - \chi_a k_y) \cosh\left(\frac{k_y d}{2}\right) + (1 + \chi_d) k_y \sinh\left(\frac{k_y d}{2}\right)} e^{\frac{1}{2}|k_y|d}.$$
 (F20)

Next, we calculate the magnetization fluctuation using

$$\delta \mathbf{M} = \begin{pmatrix} \chi_{\mathbf{d}} & -i\chi_{\mathbf{a}} & 0\\ i\chi_{\mathbf{a}} & \chi_{\mathbf{d}} & 0\\ 0 & 0 & 0 \end{pmatrix} \nabla \psi, \tag{F21}$$

yielding

$$\delta M_x = \left[\left(A \chi_{\mathbf{a}} k_y - B \chi_{\mathbf{d}} k_x^i \right) \sin(k_x^i x) + \left(A \chi_{\mathbf{d}} k_x^i + B \chi_{\mathbf{a}} k_y \right) \cos(k_x^i x) \right] e^{ik_y y} \cos(k_z z), \tag{F22}$$

$$\delta M_y = i \left[\left(A \chi_{\mathrm{d}} k_y - B \chi_{\mathrm{a}} k_x^i \right) \sin(k_x^i x) + \left(A \chi_{\mathrm{a}} k_x^i + B \chi_{\mathrm{d}} k_y \right) \cos(k_x^i x) \right] e^{ik_y y} \cos(k_z z), \tag{F23}$$

and $\delta M_z=0$. These expressions are substituted into the magnon normalization condition

leading to

$$2L_yL_zk_y(B\chi_d+iA\chi_a)(A\chi_d-iB\chi_a)\sinh(k_yd)+i\gamma\hbar M_s = 0,$$
(F25)

$$\int dV \, \boldsymbol{M}_{\mathrm{s}} \cdot (\delta \boldsymbol{M}^* \times \delta \boldsymbol{M}) = i \gamma \hbar M_{\mathrm{s}}^2, \qquad \text{(F24)} \qquad \text{where } L_y L_z \text{ denotes the cross-sectional area of the magnet.}$$

Substituting Eq. (F19) gives

$$A = -\operatorname{sgn}(k_y) \sqrt{\frac{\gamma \hbar M_s}{2S k_y \mathfrak{a}_1 \mathfrak{a}_2 \sinh(k_y d)}} \left\{ \operatorname{sgn}(k_y) \left[\chi_a + (1 + \chi_d) \tanh\left(\frac{k_y d}{2}\right) \right] + 1 \right\}, \tag{F26}$$

with

$$\begin{split} &\mathfrak{a}_1 = \left[\chi_{\mathrm{a}} - (\chi_{\mathrm{d}}^2 + \chi_{\mathrm{d}} - \chi_{\mathrm{a}}^2) \operatorname{sgn}(k_y)\right] \tanh\left(\frac{k_y d}{2}\right) + \chi_{\mathrm{a}} \operatorname{sgn}(k_y) - \chi_{\mathrm{d}}, \\ &\mathfrak{a}_2 = \left[\chi_{\mathrm{a}} \operatorname{sgn}(k_y) - \chi_{\mathrm{d}}\right] \tanh\left(\frac{k_y d}{2}\right) - (\chi_{\mathrm{d}}^2 + \chi_{\mathrm{d}} - \chi_{\mathrm{a}}^2) \operatorname{sgn}(k_y) + \chi_{\mathrm{a}}. \end{split}$$

The associated magnetic field fluctuations at the upper surface x > d/2 are given by $\delta \mathbf{H} = \nabla \psi$, yielding

$$\delta \boldsymbol{H}_{k}(\boldsymbol{r}) = \delta H_{k}(\boldsymbol{r}) \times \begin{cases} \boldsymbol{e}_{-}, & k_{y} > 0, \\ \boldsymbol{e}_{+}, & k_{y} < 0. \end{cases}$$
 (F27)

Here, we have $\delta H_k(\mathbf{r}) = \sqrt{2}Ck_ye^{-x|k_y|+ik_yy}$ (see Fig. 12). Note that we consider the single propagation direction. Thus, the subscript y in the wave number is omitted hereafter, i.e., $k_y = k$.

The magnon-qubit coupling g_k along the unidirectional axis is determined by plugging the mode profile of Eq. (F27) evaluated at the qubit position into Eq. (20). We use the dispersion in Eq. (F17) to determine the group velocity v_k and use $\mathcal{D}(k) = L_y/(2\pi)$ to determine the dissipative coupling $J_q = 2\pi \mathcal{D}(k_q)|g_{k_q}|^2/v_{k_q}$, with the parameters listed in Table I.

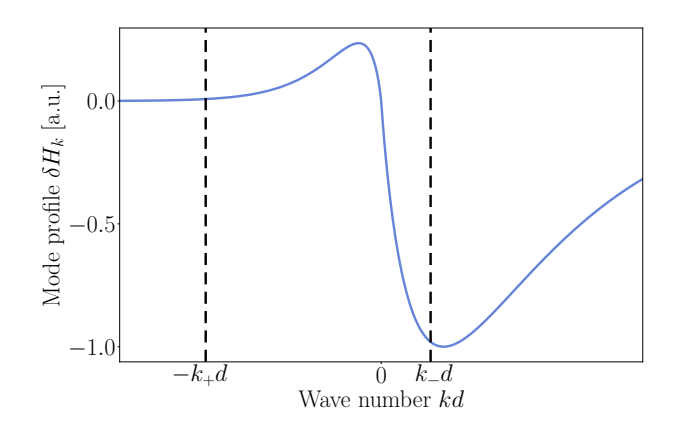


FIG. 12: Normalized mode profile δH_k as a function of the wave number k normalized by the film thickness d evaluated at $x = d_{\text{NV}} + d/2$ and y = z = 0. Due to the field displacement non-reciprocity, the mode profile has a higher amplitude for positive k than for negative k. The resonant wave numbers $-k_+$ and k_- from Fig. 7 are also shown. The parameters chosen to obtain this figure are in Table I.

- H. J. Carmichael, Quantum trajectory theory for cascaded open systems, Physical Review Letters 70, 2273 (1993).
- [2] C. W. Gardiner, Driving a quantum system with the output field from another driven quantum system, Physical Review Letters 70, 2269 (1993).
- [3] P. Lodahl, S. Mahmoodian, S. Stobbe, A. Rauschenbeutel, P. Schneeweiss, J. Volz, H. Pichler, and P. Zoller, Chiral quantum optics, Nature 541, 473 (2017).
- [4] D. Suárez-Forero, M. Jalali Mehrabad, C. Vega, A. González-Tudela, and M. Hafezi, Chiral Quantum Optics: Recent Developments and Future Directions, PRX Quantum 6, 020101 (2025).
- [5] K. Stannigel, P. Rabl, and P. Zoller, Driven-dissipative preparation of entangled states in cascaded quantumoptical networks, New Journal of Physics 14, 063014 (2012).
- [6] H. Pichler, T. Ramos, A. J. Daley, and P. Zoller, Quantum optics of chiral spin networks, Physical Review A 91, 042116 (2015).
- [7] A. Gonzalez-Tudela, D. Martin-Cano, E. Moreno, L. Martin-Moreno, C. Tejedor, and F. J. Garcia-Vidal, Entanglement of Two Qubits Mediated by One-Dimensional Plasmonic Waveguides, Physical Review Letters 106, 020501 (2011).
- [8] A. González-Tudela and D. Porras, Mesoscopic Entanglement Induced by Spontaneous Emission in Solid-State Quantum Optics, Physical Review Letters 110, 080502 (2013).
- [9] N. Gisin, G. Ribordy, W. Tittel, and H. Zbinden, Quantum cryptography, Reviews of Modern Physics 74, 145 (2002).
- [10] A. M. Steane, Error Correcting Codes in Quantum The-

- ory, Physical Review Letters 77, 793 (1996).
- [11] C. Corlett, I. Cepaitė, A. J. Daley, C. Gustiani, G. Pelegrí, J. D. Pritchard, N. Linden, and P. Skrzypczyk, Speeding Up Quantum Measurement Using Space-Time Trade-Off, Physical Review Letters 134, 080801 (2025).
- [12] M. A. Nielsen and I. L. Chuang, Quantum Computation and Quantum Information, 10th ed. (Cambridge Univ. Press, Cambridge, 2009).
- [13] I. J. Luxmoore, N. A. Wasley, A. J. Ramsay, A. C. T. Thijssen, R. Oulton, M. Hugues, S. Kasture, V. G. Achanta, A. M. Fox, and M. S. Skolnick, Interfacing Spins in an InGaAs Quantum Dot to a Semiconductor Waveguide Circuit Using Emitted Photons, Physical Review Letters 110, 037402 (2013).
- [14] I. J. Luxmoore, N. A. Wasley, A. J. Ramsay, A. C. T. Thijssen, R. Oulton, M. Hugues, A. M. Fox, and M. S. Skolnick, Optical control of the emission direction of a quantum dot, Applied Physics Letters 103, 241102 (2013).
- [15] R. Mitsch, C. Sayrin, B. Albrecht, P. Schneeweiss, and A. Rauschenbeutel, Quantum state-controlled directional spontaneous emission of photons into a nanophotonic waveguide, Nature Communications 5, 5713 (2014).
- [16] R. J. Coles, D. M. Price, J. E. Dixon, B. Royall, E. Clarke, P. Kok, M. S. Skolnick, A. M. Fox, and M. N. Makhonin, Chirality of nanophotonic waveguide with embedded quantum emitter for unidirectional spin transfer, Nature Communications 7, 11183 (2016).
- [17] I. Söllner, S. Mahmoodian, S. L. Hansen, L. Midolo, A. Javadi, G. Kiršanskė, T. Pregnolato, H. El-Ella, E. H. Lee, J. D. Song, S. Stobbe, and P. Lodahl, De-

- terministic photon-emitter coupling in chiral photonic circuits, Nature Nanotechnology 10, 775 (2015).
- [18] Z. Yang, S. Aghaeimeibodi, and E. Waks, Chiral lightmatter interactions using spin-valley states in transition metal dichalcogenides, Optics Express 27, 21367 (2019).
- [19] N. O. Antoniadis, N. Tomm, T. Jakubczyk, R. Schott, S. R. Valentin, A. D. Wieck, A. Ludwig, R. J. Warburton, and A. Javadi, A chiral one-dimensional atom using a quantum dot in an open microcavity, npj Quantum Information 8, 27 (2022).
- [20] R. Shreiner, K. Hao, A. Butcher, and A. A. High, Electrically controllable chirality in a nanophotonic interface with a two-dimensional semiconductor, Nature Photonics 16, 330 (2022).
- [21] T. P. Lyons, D. J. Gillard, C. Leblanc, J. Puebla, D. D. Solnyshkov, L. Klompmaker, I. A. Akimov, C. Louca, P. Muduli, A. Genco, M. Bayer, Y. Otani, G. Malpuech, and A. I. Tartakovskii, Giant effective Zeeman splitting in a monolayer semiconductor realized by spin-selective strong light-matter coupling, Nature Photonics 16, 632 (2022).
- [22] M. J. R. Staunstrup, A. Tiranov, Y. Wang, S. Scholz, A. D. Wieck, A. Ludwig, L. Midolo, N. Rotenberg, P. Lodahl, and H. Le Jeannic, Direct observation of a few-photon phase shift induced by a single quantum emitter in a waveguide, Nature Communications 15, 7583 (2024).
- [23] D. D. Awschalom, R. Hanson, J. Wrachtrup, and B. B. Zhou, Quantum technologies with optically interfaced solid-state spins, Nature Photonics 12, 516–527 (2018).
- [24] D. Lachance-Quirion, Y. Tabuchi, A. Gloppe, K. Usami, and Y. Nakamura, Hybrid quantum systems based on magnonics, Applied Physics Express 12, 070101 (2019).
- [25] G. Schmidt, C. Hauser, P. Trempler, M. Paleschke, and E. T. Papaioannou, Ultra Thin Films of Yttrium Iron Garnet with Very Low Damping: A Review, physica status solidi (b) 257, 1900644 (2020).
- [26] A. V. Chumak, P. Kabos, M. Wu, C. Abert, C. Adelmann, A. O. Adeyeye, J. Åkerman, F. G. Aliev, A. Anane, A. Awad, C. H. Back, A. Barman, G. E. W. Bauer, M. Becherer, E. N. Beginin, V. A. S. V. Bittencourt, Y. M. Blanter, P. Bortolotti, I. Boventer, D. A. Bozhko, S. A. Bunyaev, J. J. Carmiggelt, R. R. Cheenikundil, F. Ciubotaru, S. Cotofana, G. Csaba, O. V. Dobrovolskiy, C. Dubs, M. Elyasi, K. G. Fripp, H. Fulara, I. A. Golovchanskiy, C. Gonzalez-Ballestero, P. Graczyk, D. Grundler, P. Gruszecki, G. Gubbiotti, K. Guslienko, A. Haldar, S. Hamdioui, R. Hertel, B. Hillebrands, T. Hioki, A. Houshang, C.-M. Hu, H. Huebl, M. Huth, E. Iacocca, M. B. Jungfleisch, G. N. Kakazei, A. Khitun, R. Khymyn, T. Kikkawa, M. Kläui, O. Klein, J. W. Kłos, S. Knauer, S. Koraltan, M. Kostylev, M. Krawczyk, I. N. Krivorotov, V. V. Kruglyak, D. Lachance-Quirion, S. Ladak, R. Lebrun, Y. Li, M. Lindner, R. Macêdo, S. Mayr, G. A. Melkov, S. Mieszczak, Y. Nakamura, H. T. Nembach, A. A. Nikitin, S. A. Nikitov, V. Novosad, J. A. Otálora, Y. Otani, A. Papp, B. Pigeau, P. Pirro, W. Porod, F. Porrati, H. Qin, B. Rana, T. Reimann, F. Riente, O. Romero-Isart, A. Ross, A. V. Sadovnikov, A. R. Safin, E. Saitoh, G. Schmidt, H. Schultheiss, K. Schultheiss, A. A. Serga, S. Sharma, J. M. Shaw, D. Suess, O. Surzhenko, K. Szulc, T. Taniguchi, M. Urbánek, K. Usami, A. B. Ustinov, T. van der Sar,

- S. van Dijken, V. I. Vasyuchka, R. Verba, S. V. Kusminskiy, Q. Wang, M. Weides, M. Weiler, S. Wintz, S. P. Wolski, and X. Zhang, Advances in Magnetics Roadmap on Spin-Wave Computing, IEEE Transactions on Magnetics **58**, 1 (2022).
- [27] H. Y. Yuan, Y. Cao, A. Kamra, R. A. Duine, and P. Yan, Quantum magnonics: When magnon spintronics meets quantum information science, Physics Reports Quantum Magnonics: When Magnon Spintronics Meets Quantum Information Science, 965, 1 (2022).
- [28] B. Zare Rameshti, S. Viola Kusminskiy, J. A. Haigh, K. Usami, D. Lachance-Quirion, Y. Nakamura, C.-M. Hu, H. X. Tang, G. E. W. Bauer, and Y. M. Blanter, Cavity magnonics, Physics Reports Cavity Magnonics, 979, 1 (2022).
- [29] B. Flebus, D. Grundler, B. Rana, Y. Otani, I. Barsukov, A. Barman, G. Gubbiotti, P. Landeros, J. Akerman, U. Ebels, P. Pirro, V. E. Demidov, K. Schultheiss, G. Csaba, Q. Wang, F. Ciubotaru, D. E. Nikonov, P. Che, R. Hertel, T. Ono, D. Afanasiev, J. Mentink, T. Rasing, B. Hillebrands, S. V. Kusminskiy, W. Zhang, C. R. Du, A. Finco, T. van der Sar, Y. K. Luo, Y. Shiota, J. Sklenar, T. Yu, and J. Rao, The 2024 magnonics roadmap, Journal of Physics: Condensed Matter 36, 363501 (2024).
- [30] M. Weiler, H. Huebl, F. S. Goerg, F. D. Czeschka, R. Gross, and S. T. B. Goennenwein, Spin Pumping with Coherent Elastic Waves, Physical Review Letters 108, 176601 (2012).
- [31] X. Zhang, C.-L. Zou, L. Jiang, and H. X. Tang, Cavity magnomechanics, Science Advances 2, e1501286 (2016).
- [32] K. An, A. N. Litvinenko, R. Kohno, A. A. Fuad, V. V. Naletov, L. Vila, U. Ebels, G. de Loubens, H. Hurdequint, N. Beaulieu, J. Ben Youssef, N. Vukadinovic, G. E. W. Bauer, A. N. Slavin, V. S. Tiberkevich, and O. Klein, Coherent long-range transfer of angular momentum between magnon Kittel modes by phonons, Physical Review B 101, 060407 (2020).
- [33] C. A. Potts, E. Varga, V. A. S. V. Bittencourt, S. V. Kusminskiy, and J. P. Davis, Dynamical Backaction Magnomechanics, Physical Review X 11, 031053 (2021).
- [34] R. Schlitz, L. Siegl, T. Sato, W. Yu, G. E. W. Bauer, H. Huebl, and S. T. B. Goennenwein, Magnetization dynamics affected by phonon pumping, Physical Review B 106, 014407 (2022).
- [35] M. Müller, Chiral phonons and phononic birefringence in ferromagnetic metal-bulk acoustic resonator hybrids, Physical Review B 109, 024430 (2024).
- [36] Ö. O. Soykal and M. E. Flatté, Strong Field Interactions between a Nanomagnet and a Photonic Cavity, Physical Review Letters 104, 077202 (2010).
- [37] H. Huebl, C. W. Zollitsch, J. Lotze, F. Hocke, M. Greifenstein, A. Marx, R. Gross, and S. T. B. Goennenwein, High Cooperativity in Coupled Microwave Resonator Ferrimagnetic Insulator Hybrids, Physical Review Letters 111, 127003 (2013).
- [38] Y. Tabuchi, S. Ishino, T. Ishikawa, R. Yamazaki, K. Usami, and Y. Nakamura, Hybridizing Ferromagnetic Magnons and Microwave Photons in the Quantum Limit, Physical Review Letters 113, 083603 (2014).
- [39] X. Zhang, C.-L. Zou, L. Jiang, and H. X. Tang, Strongly Coupled Magnons and Cavity Microwave Photons, Physical Review Letters 113, 156401 (2014).

- [40] M. Goryachev, W. G. Farr, D. L. Creedon, Y. Fan, M. Kostylev, and M. E. Tobar, High-Cooperativity Cavity QED with Magnons at Microwave Frequencies, Physical Review Applied 2, 054002 (2014).
- [41] A. Osada, R. Hisatomi, A. Noguchi, Y. Tabuchi, R. Yamazaki, K. Usami, M. Sadgrove, R. Yalla, M. Nomura, and Y. Nakamura, Cavity Optomagnonics with Spin-Orbit Coupled Photons, Physical Review Letters 116, 223601 (2016).
- [42] T. Liu, X. Zhang, H. X. Tang, and M. E. Flatté, Optomagnonics in magnetic solids, Physical Review B 94, 060405 (2016).
- [43] S. Viola Kusminskiy, H. X. Tang, and F. Marquardt, Coupled spin-light dynamics in cavity optomagnonics, Physical Review A 94, 033821 (2016).
- [44] X. Zhang, N. Zhu, C.-L. Zou, and H. X. Tang, Optomagnonic Whispering Gallery Microresonators, Physical Review Letters 117, 123605 (2016).
- [45] J. A. Haigh, N. J. Lambert, S. Sharma, Y. M. Blanter, G. E. W. Bauer, and A. J. Ramsay, Selection rules for cavity-enhanced Brillouin light scattering from magnetostatic modes, Physical Review B 97, 214423 (2018).
- [46] Y. Tabuchi, S. Ishino, A. Noguchi, T. Ishikawa, R. Yamazaki, K. Usami, and Y. Nakamura, Coherent coupling between a ferromagnetic magnon and a superconducting qubit, Science 349, 405 (2015).
- [47] D. Lachance-Quirion, S. P. Wolski, Y. Tabuchi, S. Kono, K. Usami, and Y. Nakamura, Entanglement-based single-shot detection of a single magnon with a superconducting qubit, Science 367, 425 (2020).
- [48] S. P. Wolski, D. Lachance-Quirion, Y. Tabuchi, S. Kono, A. Noguchi, K. Usami, and Y. Nakamura, Dissipation-Based Quantum Sensing of Magnons with a Superconducting Qubit, Physical Review Letters 125, 117701 (2020).
- [49] M. Kounalakis, G. E. W. Bauer, and Y. M. Blanter, Analog Quantum Control of Magnonic Cat States on a Chip by a Superconducting Qubit, Physical Review Letters 129, 037205 (2022).
- [50] D. Xu, X.-K. Gu, H.-K. Li, Y.-C. Weng, Y.-P. Wang, J. Li, H. Wang, S.-Y. Zhu, and J. Q. You, Quantum Control of a Single Magnon in a Macroscopic Spin System, Physical Review Letters 130, 193603 (2023).
- [51] M. Dols, S. Sharma, L. Bechara, Y. M. Blanter, M. Kounalakis, and S. Viola Kusminskiy, Magnonmediated quantum gates for superconducting qubits, Physical Review B 110, 104416 (2024).
- [52] L. Trifunovic, F. L. Pedrocchi, and D. Loss, Long-Distance Entanglement of Spin Qubits via Ferromagnet, Physical Review X 3, 041023 (2013).
- [53] F. Casola, T. van der Sar, and A. Yacoby, Probing condensed matter physics with magnetometry based on nitrogen-vacancy centres in diamond, Nature Reviews Materials 3, 1 (2018).
- [54] B. Flebus and Y. Tserkovnyak, Entangling distant spin qubits via a magnetic domain wall, Physical Review B 99, 140403 (2019).
- [55] I. Bertelli, J. J. Carmiggelt, T. Yu, B. G. Simon, C. C. Pothoven, G. E. W. Bauer, Y. M. Blanter, J. Aarts, and T. van der Sar, Magnetic resonance imaging of spin-wave transport and interference in a magnetic insulator, Science Advances 6, eabd3556 (2020).
- [56] T. Neuman, D. S. Wang, and P. Narang, Nanomagnonic Cavities for Strong Spin-Magnon Coupling

- and Magnon-Mediated Spin-Spin Interactions, Physical Review Letters **125**, 247702 (2020).
- [57] M. Fukami, D. R. Candido, D. D. Awschalom, and M. E. Flatté, Opportunities for Long-Range Magnon-Mediated Entanglement of Spin Qubits via On- and Off-Resonant Coupling, PRX Quantum 2, 040314 (2021).
- [58] C. Gonzalez-Ballestero, T. Van Der Sar, and O. Romero-Isart, Towards a quantum interface between spin waves and paramagnetic spin baths, Physical Review B 105, 075410 (2022).
- [59] B. Hetényi, A. Mook, J. Klinovaja, and D. Loss, Long-distance coupling of spin qubits via topological magnons, Physical Review B 106, 235409 (2022).
- [60] V. Karanikolas, T. Kuroda, and J.-i. Inoue, Magnon-mediated spin entanglement in the strong-coupling regime, Physical Review Research 4, 043180 (2022).
- [61] M. Fukami, J. C. Marcks, D. R. Candido, L. R. Weiss, B. Soloway, S. E. Sullivan, N. Delegan, F. J. Heremans, M. E. Flatté, and D. D. Awschalom, Magnonmediated qubit coupling determined via dissipation measurements, Proceedings of the National Academy of Sciences 121, e2313754120 (2024).
- [62] M. Bejarano, F. J. T. Goncalves, T. Hache, M. Hollenbach, C. Heins, T. Hula, L. Körber, J. Heinze, Y. Berencén, M. Helm, J. Fassbender, G. V. Astakhov, and H. Schultheiss, Parametric magnon transduction to spin qubits, Science Advances 10, eadi2042 (2024).
- [63] M.-L. Peng, M. Tian, X.-C. Chen, M.-F. Wang, G.-Q. Zhang, H.-C. Li, and W. Xiong, Cavity magnon-polariton interface for strong spin-spin coupling, Optics Letters 50, 1516 (2025).
- [64] Z. Xue, J. Zou, C. Cai, G. E. W. Bauer, and T. Yu, Directional entanglement of spin-orbit locked nitrogenvacancy centers by magnons (2025), arXiv:2505.07325.
- [65] R. W. Damon and J. R. Eshbach, Magnetostatic modes of a ferromagnet slab, Journal of Physics and Chemistry of Solids 19, 308 (1961).
- [66] J. P. Parekh, K. W. Chang, and H. S. Tuan, Propagation characteristics of magnetostatic waves, Circuits, Systems and Signal Processing 4, 9 (1985).
- [67] L. Udvardi and L. Szunyogh, Chiral Asymmetry of the Spin-Wave Spectra in Ultrathin Magnetic Films, Physical Review Letters 102, 207204 (2009).
- [68] D. Cortés-Ortuño and P. Landeros, Influence of the Dzyaloshinskii-Moriya interaction on the spin-wave spectra of thin films, Journal of Physics: Condensed Matter 25, 156001 (2013).
- [69] M. Belmeguenai, J.-P. Adam, Y. Roussigné, S. Eimer, T. Devolder, J.-V. Kim, S. M. Cherif, A. Stashkevich, and A. Thiaville, Interfacial Dzyaloshinskii-Moriya interaction in perpendicularly magnetized ${\rm Pt/Co/AlO}_x$ ultrathin films measured by Brillouin light spectroscopy, Physical Review B **91**, 180405 (2015).
- [70] S. Tacchi, R. E. Troncoso, M. Ahlberg, G. Gubbiotti, M. Madami, J. Åkerman, and P. Landeros, Interfacial Dzyaloshinskii-Moriya Interaction in Pt/CoFeB Films: Effect of the Heavy-Metal Thickness, Physical Review Letters 118, 147201 (2017).
- [71] R. A. Gallardo, D. Cortés-Ortuño, T. Schneider, A. Roldán-Molina, F. Ma, R. E. Troncoso, K. Lenz, H. Fangohr, J. Lindner, and P. Landeros, Flat Bands, Indirect Gaps, and Unconventional Spin-Wave Behavior Induced by a Periodic Dzyaloshinskii-Moriya Interaction, Physical Review Letters 122, 067204 (2019).

- [72] J. A. Otálora, M. Yan, H. Schultheiss, R. Hertel, and A. Kákay, Curvature-Induced Asymmetric Spin-Wave Dispersion, Physical Review Letters 117, 227203 (2016).
- [73] L. Körber, R. Verba, J. A. Otálora, V. Kravchuk, J. Lindner, J. Fassbender, and A. Kákay, Curvilinear spin-wave dynamics beyond the thin-shell approximation: Magnetic nanotubes as a case study, Physical Review B 106, 014405 (2022).
- [74] B. Hillebrands, Spin-wave calculations for multilayered structures, Physical Review B 41, 530 (1990).
- [75] Kh. Zakeri, Y. Zhang, J. Prokop, T.-H. Chuang, N. Sakr, W. X. Tang, and J. Kirschner, Asymmetric Spin-Wave Dispersion on Fe(110): Direct Evidence of the Dzyaloshinskii-Moriya Interaction, Physical Review Letters 104, 137203 (2010).
- [76] R. A. Gallardo, P. Alvarado-Seguel, T. Schneider, C. Gonzalez-Fuentes, A. Roldán-Molina, K. Lenz, J. Lindner, and P. Landeros, Spin-wave non-reciprocity in magnetization-graded ferromagnetic films, New Journal of Physics 21, 033026 (2019).
- [77] R. Gallardo, T. Schneider, A. Chaurasiya, A. Oelschlägel, S. Arekapudi, A. Roldán-Molina, R. Hübner, K. Lenz, A. Barman, J. Fassbender, J. Lindner, O. Hellwig, and P. Landeros, Reconfigurable Spin-Wave Nonreciprocity Induced by Dipolar Interaction in a Coupled Ferromagnetic Bilayer, Physical Review Applied 12, 034012 (2019).
- [78] R. Gallardo, M. Weigand, K. Schultheiss, A. Kakay, R. Mattheis, J. Raabe, G. Schütz, A. Deac, J. Lindner, and S. Wintz, Coherent Magnons with Giant Nonreciprocity at Nanoscale Wavelengths, ACS Nano 18, 5249 (2024).
- [79] C. Heins, V. Iurchuk, O. Gladii, L. Körber, A. Kákay, J. Fassbender, K. Schultheiss, and H. Schultheiss, Nonreciprocal spin-wave dispersion in magnetic bilayers, Physical Review B 111, 134434 (2025).
- [80] S. Wintz, V. Tiberkevich, M. Weigand, J. Raabe, J. Lindner, A. Erbe, A. Slavin, and J. Fassbender, Magnetic vortex cores as tunable spin-wave emitters, Nature Nanotechnology 11, 948 (2016).
- [81] V. Sluka, T. Schneider, R. A. Gallardo, A. Kákay, M. Weigand, T. Warnatz, R. Mattheis, A. Roldán-Molina, P. Landeros, V. Tiberkevich, A. Slavin, G. Schütz, A. Erbe, A. Deac, J. Lindner, J. Raabe, J. Fassbender, and S. Wintz, Emission and propagation of 1D and 2D spin waves with nanoscale wavelengths in anisotropic spin textures, Nature Nanotechnology 14, 328 (2019).
- [82] M. Ishibashi, Y. Shiota, T. Li, S. Funada, T. Moriyama, and T. Ono, Switchable giant nonreciprocal frequency shift of propagating spin waves in synthetic antiferromagnets, Science Advances 6, eaaz6931 (2020).
- [83] G. Thiancourt, S. Ngom, N. Bardou, and T. Devolder, Unidirectional spin waves measured using propagatingspin-wave spectroscopy, Physical Review Applied 22, 034040 (2024).
- [84] O. Wojewoda, J. Holobrádek, D. Pavelka, E. Pribytova, J. Krčma, J. Klíma, J. Panda, J. Michalička, T. Lednický, A. V. Chumak, and M. Urbánek, Unidirectional propagation of zero-momentum magnons, Applied Physics Letters 125, 132401 (2024).
- [85] J. R. Weber, W. F. Koehl, J. B. Varley, A. Janotti, B. B. Buckley, C. G. Van de Walle, and D. D. Awschalom,

- Quantum computing with defects, Proceedings of the National Academy of Sciences 107, 8513 (2010).
- [86] M. W. Doherty, N. B. Manson, P. Delaney, F. Jelezko, J. Wrachtrup, and L. C. L. Hollenberg, The nitrogenvacancy colour centre in diamond, Physics Reports The Nitrogen-Vacancy Colour Centre in Diamond, 528, 1 (2013).
- [87] R. O. Serha, K. H. McAllister, F. Majcen, S. Knauer, T. Reimann, C. Dubs, G. A. Melkov, A. A. Serga, V. S. Tyberkevych, A. V. Chumak, and D. A. Bozhko, Ultra-long-living magnons in the quantum limit (2025), arXiv:2505.22773.
- [88] L. Viola, E. Knill, and S. Lloyd, Dynamical Decoupling of Open Quantum Systems, Physical Review Letters 82, 2417 (1999).
- [89] N. Bar-Gill, L. M. Pham, A. Jarmola, D. Budker, and R. L. Walsworth, Solid-state electronic spin coherence time approaching one second, Nature Communications 4, 1743 (2013).
- [90] A. Metelmann and A. A. Clerk, Nonreciprocal Photon Transmission and Amplification via Reservoir Engineering, Physical Review X 5, 021025 (2015).
- [91] H.-P. Breuer and F. Petruccione, The Theory of Open Quantum Systems, 1st ed. (Oxford University PressOxford, 2007).
- [92] F. Minganti, A. Miranowicz, R. W. Chhajlany, and F. Nori, Quantum exceptional points of non-Hermitian Hamiltonians and Liouvillians: The effects of quantum jumps, Physical Review A 100, 062131 (2019).
- [93] L. Brundle and N. Freedman, Magnetostatic surface waves on a y.i.g. slab, Electronics Letters 4, 132 (1968).
- [94] T. Wolfram and R. E. DeWames, Surface dynamics of magnetic materials, Progress in Surface Science 2, 233 (1972).
- [95] E. D. Herbschleb, H. Kato, Y. Maruyama, T. Danjo, T. Makino, S. Yamasaki, I. Ohki, K. Hayashi, H. Morishita, M. Fujiwara, and N. Mizuochi, Ultra-long coherence times amongst room-temperature solid-state spins, Nature Communications 10, 3766 (2019).
- [96] V. Cherepanov, I. Kolokolov, and V. L'vov, The saga of YIG: Spectra, thermodynamics, interaction and relaxation of magnons in a complex magnet, Physics Reports 229, 81 (1993).
- [97] F. Dolde, I. Jakobi, B. Naydenov, N. Zhao, S. Pezza-gna, C. Trautmann, J. Meijer, P. Neumann, F. Jelezko, and J. Wrachtrup, Room-temperature entanglement between single defect spins in diamond, Nature Physics 9, 139 (2013).
- [98] I. Arrazola, P. Bertet, Y. Chu, and P. Rabl, Engineering protected cavity-QED interactions through pulsed dynamical decoupling (2025), arXiv:2505.02929.
- [99] G. Burkard, T. D. Ladd, A. Pan, J. M. Nichol, and J. R. Petta, Semiconductor spin qubits, Reviews of Modern Physics 95, 025003 (2023).
- [100] M. Kim, A. Tabesh, T. Zegray, S. Barzanjeh, and C.-M. Hu, Nonreciprocity in cavity magnonics at millikelvin temperature, Journal of Applied Physics 135, 063904 (2024).
- [101] M. Hiraishi, Z. H. Roberts, G. G. G. King, L. S. Trainor, and J. J. Longdell, Long optical coherence times in a rare-earth-doped antiferromagnet, Nature Physics , 1 (2025).
- [102] D. García-Pons, J. Pérez-Bailón, C. Boix-Constant, I. Gómez-Muñoz, X. del Arco, S. Mañas-Valero,

- E. Coronado, D. Zueco, and M. J. Martínez-Pérez, Strong spin-magnon coupling in a van der Waals magnet with tunable chiral symmetry (2025), arXiv:2508.17888 [quant-ph].
- [103] J. N. Greiner, D. B. R. Dasari, and J. Wrachtrup, Purification of an unpolarized spin ensemble into entangled singlet pairs, Scientific Reports 7, 10.1038/s41598-017-00603-z (2017).
- [104] N. Y. Yao, Z.-X. Gong, C. R. Laumann, S. D. Bennett, L.-M. Duan, M. D. Lukin, L. Jiang, and A. V. Gorshkov, Quantum logic between remote quantum registers, Phys. Rev. A 87, 022306 (2013).
- [105] W. Chen, c. Kaya Özdemir, G. Zhao, J. Wiersig, and

- L. Yang, Exceptional points enhance sensing in an optical microcavity, Nature **548**, 192–196 (2017).
- [106] C. Liang, Y. Tang, A.-N. Xu, and Y.-C. Liu, Observation of exceptional points in thermal atomic ensembles, Phys. Rev. Lett. 130, 263601 (2023).
- [107] R. H. Lehmberg, Radiation from an \$N\$-Atom System. I. General Formalism, Physical Review A 2, 883 (1970).
- [108] C. Vega, A. M. de las Heras, D. Porras, and A. González-Tudela, Topological, multi-mode amplification induced by non-reciprocal, long-range dissipative couplings (2025), arXiv:2405.10176.
- [109] D. D. Stancil and A. Prabhakar, Spin Waves: Theory and Applications (Springer, New York, 2009).